國立交通大學
電子物理研究所
碩士論文

圓盤狀氮化鎵自組性量子點之結構與光譜研究

Structure and optical spectroscopy studies of self-organized disk-like GaN dots

研 究 生：黃佳進
指導教授：周武清 教授

中華民國九十四年七月

圓盤狀氮化鎵自組性量子點之結構與光譜研究

Structure and optical spectroscopy studies of self-organized disk-like GaN dots

研 究 生：黃佳進　　Student： Chia-Chin Huang

指導教授：周武清 教授　　Advisor： Prof. Wu-Ching Chou

國立交通大學

電子物理研究所

碩士論文

A Thesis Submitted to
The Institute of Electrophysics
College of Science
National Chiao Tung University
In Partial Fulfillment of the Requirements
For the Degree of Master
In Electrophysics
July 2005
Hsinchu, Taiwan, Republic of China

中華民國九十四年七月

圓盤狀氮化鎵自組性量子點之結構與光譜研究

研究生：黃佳進　　指導教授：周武清 教授

國立交通大學電子物理研究所碩士班

中文摘要

本論文中我們利用原子力顯微術和光激螢光光譜來研究氮化鎵量子點結構和光學特性。從原子力顯微鏡的觀察，我們發現量子點的形狀是圓盤狀。這些量子點的尺寸隨著 TMGa 的流率增加而變大。除此之外，我們還發現在成長量子點的時候，氮化鎵磊晶層必須累積到一定的厚度之後才會形成量子點。因此我們認為利用流率調制磊晶技術所成長的量子點是透過 Stranski-Krastanow (SK)成長模式。從量子點的密度對磊晶層厚度之關係可以推估出濕潤層的厚度大約 7.2 個原子層。光激螢光光譜研究顯示量子點的躍遷能量隨著尺寸增加而變小。相對於室溫氮化鎵塊材譜峰位置有 36 到 62 毫電子伏特的藍移量。這

個藍移現象是來自量子尺寸效應所致。由變溫螢光光譜，我們發現在低溫時譜峰會隨著溫度的增加而藍移。隨著溫度繼續增加，才會跟隨著瓦希尼(Varshni) 公式所預測的紅移。而且在低溫時的藍移量會隨著量子點尺寸的增加而變大。這樣的藍移現象是以 SK 模式成長的量子點特徵，在其他的量子點系統都被觀察到。但是目前為止，在氮化鎵量子點系統中並沒有文獻上報導過此現象。我們認為在低溫時激子被侷限在量子點內的缺陷態，隨著溫度增加而游離到量子點的自由激子態，再進一步提高溫度，則自由激子克服量子點能障而熱活化到氮化鋁鎵緩衝層的缺陷態上。

Structure and optical spectroscopy studies of self-organized disk-like GaN dots

Student: Chia-Chin Huang Advisor: Dr. Wu-Ching Chou

Institute of Electrophysics

National Chiao Tung University

Abstract

In this study, structural and optical properties of self-organized GaN dots grown on $Al_{0.11}Ga_{0.89}N$/sapphire by metal organic chemical vapor deposition (MOCVD) were investigated by means of atomic force microscopy (AFM) and photoluminescence (PL) spectroscopy. AFM studies showed the disk-like shapes of GaN dots. The disk-like dot size varies with the flow rate of TMGa. We found that the formation of disk-like GaN dots starts when the average GaN coverage exceeds 7.2 MLs. It implies that the growth of disk-like GaN dots is mainly through the Stranski-Krastanow (SK) growth mode. And the wetting layer (WL) thickness is estimated to be about 7.2 MLs from the dependence of the dot density on the GaN coverage. The PL peak energy was found to decrease as the dot size increases. The blue shift is about 36 to 62 meV at room temperature in comparison with GaN epilayers. This observation is ascribed to the quantum size effect. The temperature dependent PL peak energy exhibits an initial blue-shift with increasing temperature and then followed by a red-shift which obeys the

Vashini’s relation. The strength of blue-shifts increases with dot size. Such an energy shift with increasing temperature is a signature of QDs grown by SK growth mode and has also been observed in other QDs systems except for GaN QDs. This is a typical characteristic of the exciton localization. Exciton bound to the defect state in the dots and carrier thermalization from confined well states into the defect state of buffer layer were used to explain the temperature dependent PL results.

誌　謝

歲月時轉，兩年的碩士生活，是我求學生涯中收穫最多的一段，對很多有關待人處事、研究精神及人生方面有更深一層的領悟，而在此求學的過程之中，一直抱持著不服輸的精神，實現心中的夢想。本論文得以完成，必須要感謝許多人。

首先，要由衷的感謝周武清老師、陳衛國老師、李明知老師、陳文雄老師這兩年來的指導和照顧，讓我成長許多。特別要感謝指導教授周武清老師在實驗研究以及論文寫作上，給予我耐心的指導與協助，提供我良好的研究設備與環境，並啟發我在研究觀點上的思考邏輯，使我能順利地完成論文，許許多多的指導和建議，讓我對於事情有更深一層的看法。另外，要感謝柯文正學長提供量測所需的樣品以及傳授相關的長晶知識，感謝古慶順學長在研究上的協助，以及感謝實驗室學長們，李寧、張富欽、陳京玉、院繼祖、傅振邦、蔡文哲、何志偉、顏國錫學長的指導與愛護。同時要謝謝實驗室同學鍾逸、碧軒、承勳、信志、逸文及學弟們在課業上的討論與生活上的照應，也因與你們相處而豐富了我的碩士生涯。

最後，我更要感謝我的家人和女友，感謝你們的付出、支持與鼓勵，讓我順利地完成我的學業。

在此謹將本篇論文及所有的榮耀獻給我最敬愛的父母。

平常缺少壓力的人生活過的比較悠

有壓力的人生活比較積極緊湊

同理可知，有夢想的人一定比沒有夢想的人堅強

實現夢想的途中沒有人可以難為你

就怕你自己難為你自己

有夢的人最美，勇敢做一個有夢的人

夢想所以會實現，是因為你從來不想放棄

Index

Chapter 1 Introduction

Recently, there has been much interest in the study of nitride semiconductors [1–4]. So far, the efforts were focused on the understanding of the basic material properties of the nitride family as well as the realization of various optoelectronic device fabrications. Nitride semiconductors have wide range of band gaps which allow the emission wavelengths cover the whole visible spectrum and also ultra violet (UV) light. Nakamura and co-workers [5–14] have pioneered the development of GaN-based light-emitting diodes (LEDs) which emit in a wide range of wavelengths from yellow to UV. These light sources have applications in full color display technology. Blue and UV laser diodes (LDs) are also key devices for the applications in high-density optical storage. On the other hand, nitride semiconductors are also good candidates for the high power and high temperature electronic devices due to the excellent thermal and chemical stability. Khan et al. [15, 16] have fabricated GaN-based field-effect transistors (FETs) and an AlGaN/GaN modulation-doped FET in which the existence of interfacial two-dimensional electron gas was shown. Furthermore, UV detectors, which have application in national defense, were fabricated based on GaN wide-band-gap semiconductor [17].

Low dimensional heterostructures have the advantage of strong carrier quantum confinement which gives rise to a robust electron and hole Coulomb interaction. The strong Coulomb interaction results in a stable excitonic emission at high temperature. It is essential for the light emitting devices of high brightness operated at high temperature. In addition, low dimensional heterostructures have unique density of state. Theoretical prediction shows that the light-emitting diodes (LEDs) or laser diodes (LDs) made of quantum dots (QDs) in the active layer could lead to low threshold current and weak temperature dependence for the threshold current [18]. Moreover, the self-organized

quantum dot is expected to be defect-free. As a result, carriers confined inside the QDs could avoid the nonradiative recombination centers formed by dislocations outside [19]. Usually, the practical observation of zero dimensional (0 D) confinement effect in semiconductors requires a size of less than 10 nm in all three dimensions. The first pioneering work in this field used the lithographic patterning to fabricate QDs. However, this approach is practically abandoned today because of the damage caused by the lithographic processing on the lateral walls of QD. The damage seriously degrades the optical quality of the QD devices. By contrast, self-organization resulting from the Stranski-Krastanov growth mode was proven to be very successful in achieving nanostructures with excellent 0D optical properties. In this growth mode, deposition of a strained 2D wetting layer is followed by the strain relaxation through a 3D island formation which results in the growth of defect-free QDs [20]. It has been observed for various material systems grown under compressive stress, such as GaN on $Al_xGa_{1-x}N$ [21], InAs on GaAs [22], InP on $Ga_xIn_{1-x}P$ [23]. The successful QD fabrication opens the way to achieve highly efficient lasers based on self-organized $In_xGa_{1-x}As$/GaAs [24, 25] and InAs/GaAs QDs [26, 27].

Among the QD systems, GaN quantum dots (QDs) attracted significant attention due to its promising application in UV-LEDs or LDs. Progress in GaN technology leads great accomplishment in the fabrication and characterization of different kinds of GaN QDs [28–38]. Molecular beam epitaxial growth in the Stranski–Krastanow mode of wurtzite (WZ) GaN/AlN [28-30] and GaN/$Al_xGa_{1-x}N$ [31] QDs has been reported. On the other hand, MOCVD growth was also proved to be an alternative for the growth of WZ GaN/AlN [32] and GaN/$Al_xGa_{1-x}N$ [21, 33, and 34]. Other types of WZ GaN QDs have been fabricated by pulsed laser ablation of pure Ga metal in flowing N2 gas [35], and by sequential ion implantation of Ga^+ and N^+ ions into dielectrics [36]. Also, self-organized growth of zincblende (ZB) GaN/AlN QDs has been reported [37, 38]. In

addition to the fabrication and optical characterization of WZ GaN/AlN and $GaN/Al_xGa_{1-x}N$ as well as ZB GaN/AlN QDs, there were intensive theoretical investigations of electronic states and excitonic properties of GaN QDs [39-41].

Base on the important application and interesting physical properties of GaN QDs, we have challenged the fabrication difficulty of GaN QD and successfully grown self-assembled GaN dots on $Al_{0.11}Ga_{0.89}N$/sapphire substrate using flow-rate modulation epitaxy (FME) growth technique in MOCVD system. The growth and structural properties of our self-assembled dots have been reported elsewhere [21]. In this thesis, we will discuss the structural and optical properties of self-assembled GaN dots by means of atomic force microscopy (AFM) and photoluminescence (PL) spectroscopy. AFM studies show the disk-like shapes of GaN dots. Size-dependent PL spectra of GaN dots were studied. The emission peak energy of GaN dots was observed to shift to higher energy with decreasing quantum dot size. The blue shift is about 36 to 62 meV at room temperature in comparison with GaN epilayers. In addition, the temperature dependent PL spectra were investigated to extract the activation energy from the Arrhenius plot for the understanding of thermal stability and exciton localization.

There are total of five chapters in this thesis. In Chapter 1, we introduced the studies of GaN. Theoretical background was briefly described in Chapter 2. In Chapter 3, sample structure, growth method, experimental setup as well as operation procedures were presented. In Chapter 4, we discussed the results of morphology investigation, size- and temperature-dependent micro-PL spectra of GaN dots and proposed a reasonable explanation. Finally, in Chapter 5, we summarized the significant points obtained from this study.

Chapter 2 Theoretical background

As the laser beam irradiates on a semiconductor, electrons and holes can be generated if the photon energy is larger than the semiconductor band gap. The electrons and holes may be scattered and then redistribute near the conduction band minimum and the valence band maximum, through the process of carrier-phonon interaction. Under the quasi-thermal equilibrium, electron and hole attract each other by Coulomb interaction to form free exciton. Finally, electron and hole may recombine and carry out excitonic emission. If the defects or impurities exist in the semiconductors, the electron-hole pairs may be attracted by the defects or impurities to produce defect or impurity bound excitons. In some caes, defects and impurities may play "non-radiative centers", at which the electrons or holes are absorbed but do not emit photons, so that the emission efficiency will be reduced as the number of non-radiative center increases. Two types of recombination are described as follows:

(A) Radiative transition

(I) Band to Band transition

In perfect semiconductors, the excited electrons and holes will accumulate at the conduction band minimum and valence band maximum. As shown in Fig. 2-1, electron-hole (e-h) pairs will recombine radiatively with high efficiency (in the direct band gap semiconductor). The recombination rate can be expressed as:

$$R = \int R(h\nu)d(h\nu) \sim np.$$

The recombination rate is proportional to the product of electron (n) and hole (p) concentration. But in the indirect band gap semiconductors, the transition must involve an additional particle – "phonon" (in order to satisfy the momentum conservation rule). Thus, the transition probability will be reduced, and the emission efficiency is lower

than the direct band gap semiconductors. Most of Ⅲ-Nitrides (such as GaN、InGaN、AlGaN) are direct band gap semiconductors.

(II) Exciton transition

In high quality semiconductors, the Coulomb interaction between the conduction band electrons and the valence band holes will result in the formation of the bound electron-hole pairs, that is called " exciton ". The exciton is analogous to "positron atom" – an electron bound to a positron, and this quasi-particle (exciton) is electrically neutral. In most Ⅱ-Ⅳ、Ⅲ-Ⅴ semiconductors, the exciton radius (Bohr radius) is large in comparison with the length of the lattice unit cells, they are called " Wannier excitons ". On the other hand, if the radius of the excitons is on the order of or smaller than an atomic unit cell, the excitons are called " Frenkel excitons ". In this study, the excitonic transition of GaN dots were studied by PL

(III) Donor acceptor pair recombination (DAP)

The impurities present in the semiconductors may form the donor (positive) or the acceptor (negative) levels in the energy gap. The electrons and holes created by the laser excitation may be bound to the donor (D^+) and the acceptor (A^-) to form the neutral donor (D^0) and acceptor (A^0). If the neutral donor electron and the acceptor hole recombine, as expressed by:

$$D^0 + A^0 \rightarrow h\mu + D^+ + A^-.$$

It can emit photon with an energy as described by the following formula:

$$E_{DAP} = h\mu = E_g - (E_D + E_A) + \frac{e^2}{\varepsilon \cdot R_{DA}}.$$

Where, E_g is the energy gap of semiconductor, E_D and E_A are the respective energy separation from donor level to conduction band minimum and from acceptor level to valence band maximum. R_{DA} is the distance between the donor and the acceptor. If the R_{DA} increases, the transition probability will reduce, so does the PL intensity.

(B) Non-radiative transition

There are several transitions that compete with the radiative transition and thus reduce the emission efficiency. They are depicted as follows:

(I) The e-h pair is scattered by the phonon or carriers and loses its energy.

(II) The e-h pair recombines at defect, dislocation, grain boundary or surface, and loses its excess energy, the so-called “cascade process”.

(III) The e-h pair loses its energy via the “Auger process ” that involves the core level transitions.

All the non-radiation transitions will compete with radiation transitions, the more the non-radiation transition, the lower the PL intensity.

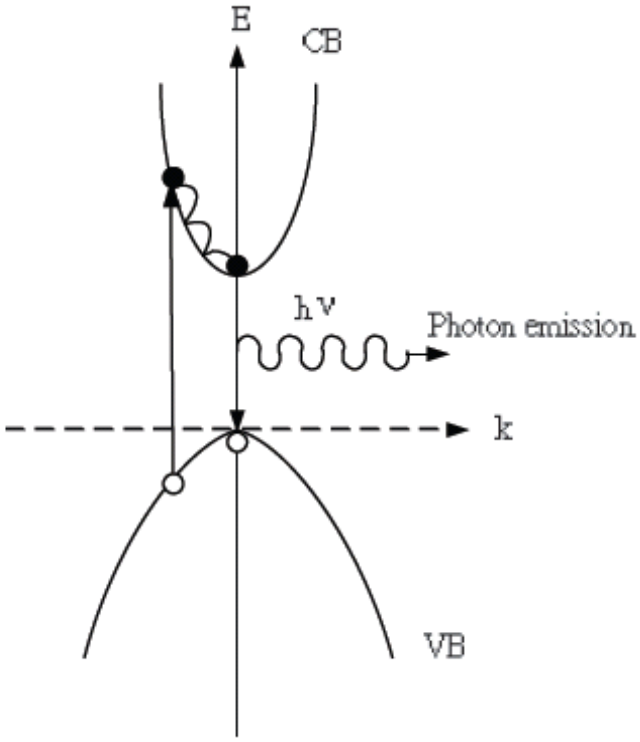

(a) Direct transition

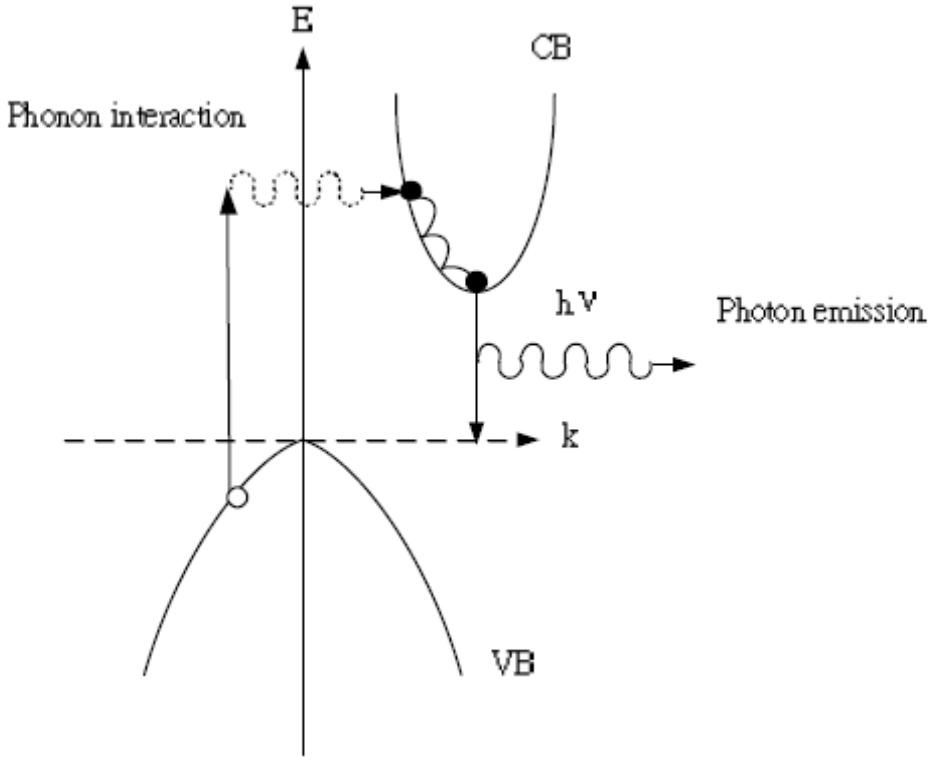

(b) Indirect transition

Fig. 2-1 Schematic representations for the (a) direct and (b) indirect transition.

Chapter 3 Experiment

In this chapter, we describe the sample preparation of the self-assembled disk-like GaN dots, the measurements of atomic force microscopy (AFM) as well as the experiment of micro-photoluminescence (μ-PL).

3.1 Sample preparations

The uncapped and capped GaN dots were grown on $Al_{0.11}Ga_{0.89}N$/sapphire (0001) substrates by AIX 200/4 RF-S horizontal-reactor MOVPE system. Trimethylgallium (TMGa), trimethylaluminum (TMAl), and ammonia (NH_3) were used as the source precursors of Ga, Al, and N, respectively. Hydrogen was used as a carrier gas. Prior to the material growth, the sapphire substrate was heated to 1120℃ in a H_2 ambient for 10 min to remove any residual impurities on the surface. The substrate was then cooled to 650℃ for the deposition of a nominal 25-nm-thick AlN nucleation layer. It followed by an increasing of substrate temperature to 1120℃ and then a growth of a 1.5 μm $Al_{0.11}Ga_{0.89}N$ layer. Finally, the GaN dots were deposited at temperature 900℃ by the flow-rate modulation epitaxy (FME) technique. Basically, the gas flow sequences for each FME cycle consist of four steps: 3 s of Ga source, 5 s of purge step, 10 s of NH_3 source and another 5 s of purge step. A total 7 cycles were grown for all samples discussed here. The change of GaN average coverage was controlled by the TMGa flow rate. The average size and density of the GaN dots varied with the average coverage. More detail about the sample growth was reported previously [21]. The sample parameters were listed in Table I. Samples A to H were grown without capping layer for the AFM investigation. A schematic diagram of the sample structure was shown in Fig. 3-1(a). In order to passivate the surface of GaN dots for the photoluminescence experiments, samples F', G', and H' were capped with a 30nm $Al_{0.11}Ga_{0.89}N$ layer on top

of the GaN dots, as shown in Fig.3-1(b).

Table I. Sample parameters.

Sample	A	B	C	D	E	F	F'	G	G'	H	H'
Capping	No	No	No	No	No	No	Yes	No	Yes	No	Yes
TMGa flow rate (sccm)	0	1	3	4	4.5	5	5	6	6	7.5	7.5
GaN coverage (MLs)	0	1.8	5.5	7.3	8.2	9.1	9.1	10.9	10.9	13.6	13.6
Average dot height/width (nm)	--	--	--	5.7 / 175	6.3 / 181	6.6 / 190	--	7.1 / 200	--	8.2 / 215	--
Aspect Ratio (height/width)	--	--	--	1/30	1/29	1/29	--	1/28	--	1/26	--
Dot density (cm^{-2})	--	--	--	$2.3x10^{8}$	$6.2x10^{8}$	$9.1x10^{8}$	--	$1.1x10^{9}$	--	$7.2x10^{8}$	--

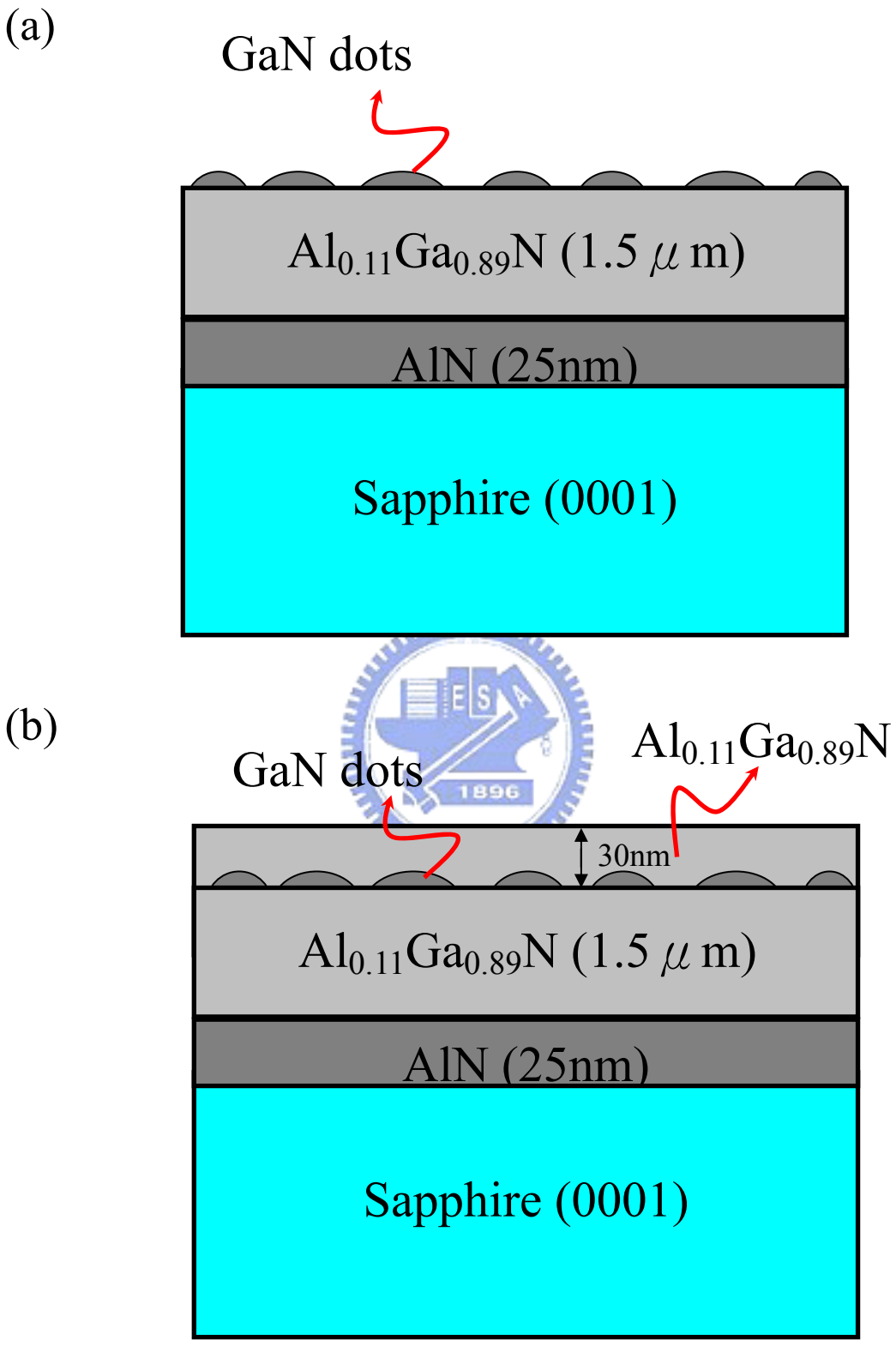

Fig. 3-1 Schematic diagrams of sample structure (a) without capping, (b) with capping layers.

3.2 Atomic Force Microscopy (AFM) System

As shown in Fig. 3-2, an atomic force microscope (AFM) is used to probe the morphology of sample surface by a sharp tip located at the free end of a flexible cantilever attached to the scanner. The interaction force between the tip and the sample surface causes the deflection of the cantilever. During scanning, the detection system measures the cantilever deflection from its initial position and then sends a signal proportional to the deflection value to the scanner control system. The signal is used to move the probe up or down by the piezo-electric crystal to bring the parameter back to its original value. Simultaneously, the probe displacement value is input to the PC memory and interpreted as the sample topography.

The scanner controls two independent movements of the cantilever: scanning along the sample surface (in X, Y plane) and movement perpendicular to the surface (along the Z-axis). The scanner is made of the piezoelectric material that expands or shrinks depending upon the sign of electrical voltage applied to it and proportionally to its value. AFM head can utilize two scanner modifications with certain design variations and different maximum scanning area capabilities: 50-micron and 90-micron. Scanner consists of two piezotubes, which have different diameters, one of which is inserted into the other. The lower end of the large tube is attached to the AFM head, with the upper part attached to the smaller diameter tube. The lower end of the latter is fixed to the cantilever holder. The smaller diameter piezoelectric tube scans in the plane parallel to the sample surface (X, Y). For the larger diameter tube, it makes the cantilever to move perpendicular the surface (along the Z-axis).

Our Scanning Probe microscopy (SPM) system was manufactured by Molecular Devices and Tools for Nano Technology (NT-MDT) in Russia. The model of AFM system was Solver P47H, that can be operated in multi-modes, such as AFM for morphology measurements, lateral force microscopy for the friction distribution , and

MFM, EFM, SKM, etc. The AFM tips were also made by NT-MDT. They have a cantilever of about 50 or 80 μm long, and a sharp tip with a radius of curvature about 10 nm. In this thesis, an AFM system was mainly used to investigate the morphology, the size distribution and dot density of the self-assembled disk-like GaN dots.

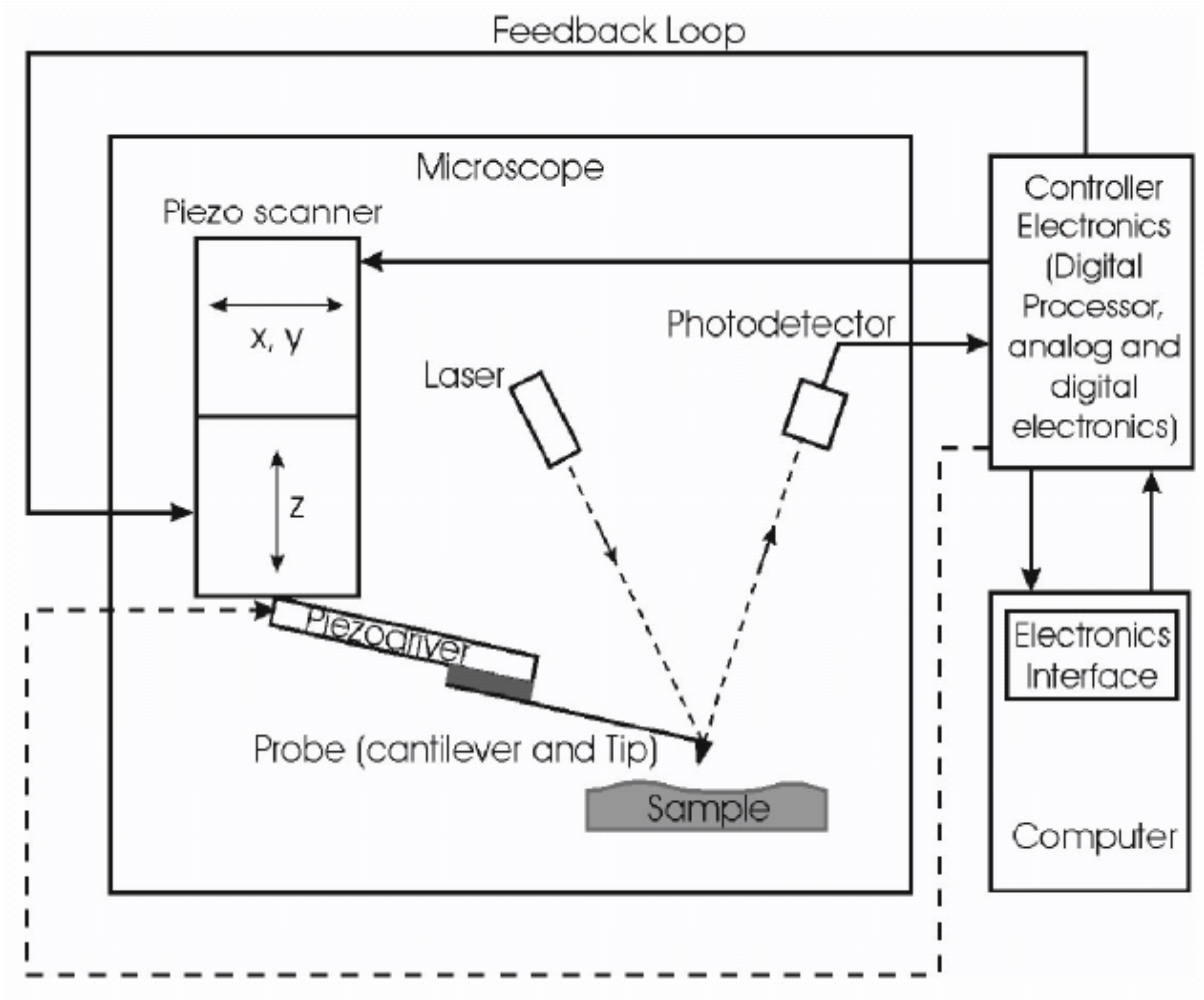

Fig. 3-2 Schematic diagram of AFM system.

3.3 Micro-photoluminescence (μ -PL) system

The micro-PL system incorporated an Olympus BH2 optical microscope. A schematic of set-up is shown in Fig. 3-3. A He-Cd laser (Omnichrome 2074-M-A02) operating at the 325nm UV line is used as the excitation light source. The output power of laser is 20 mW. The beam was reflected by two UV mirrors and then incident into the microscope, passing through a beam splitter and focused by the near-UV objective lens set (Mitutoyo NUV 100X, N.A.= 0.5). The focused spot is detected by a color CCD camera (Sony Exwave HAD), with a diameter $\leqq$ 3 μm. The PL detection system includes a collecting lens and a triple-grating monochromator (ARC Spectro PRO-500) equipped with a photomultipier tube (Hamamatsu R955), along with a photon counter (Hamamatsu C1230) for detection. The luminescence signals from the laser beam were collected by the objective lens, and then reflected by the beam splitter, through the long pass filter to cut off the laser signals. Finally, the PL signals were sent into the optical fiber, and dispersed by the monochrometer and detected by PMT. The normal applied voltage of PMT is 1000 V. When the entrance and exit slits are both opened to 50 μm, the resolution is about 0.2 nm. Moreover, we used a standard of spectral irradiance (Model 220C Optronic Laboratories) to calibrate the combined spectral response of spectrometer and detector. All signals were processed by the LabVIEW-based software.

Low-temperature μ -PL measurements were carried out using a closed cycle cryogenic system (APD HC-2D). The temperature is varied from 10 K to 300 K by the Lakeshore 330 temperature controller. In this thesis, we will investigate the size dependent quantum confinement effect and temperature-dependent PL of the disk-like GaN dots by means of PL spectroscopy.

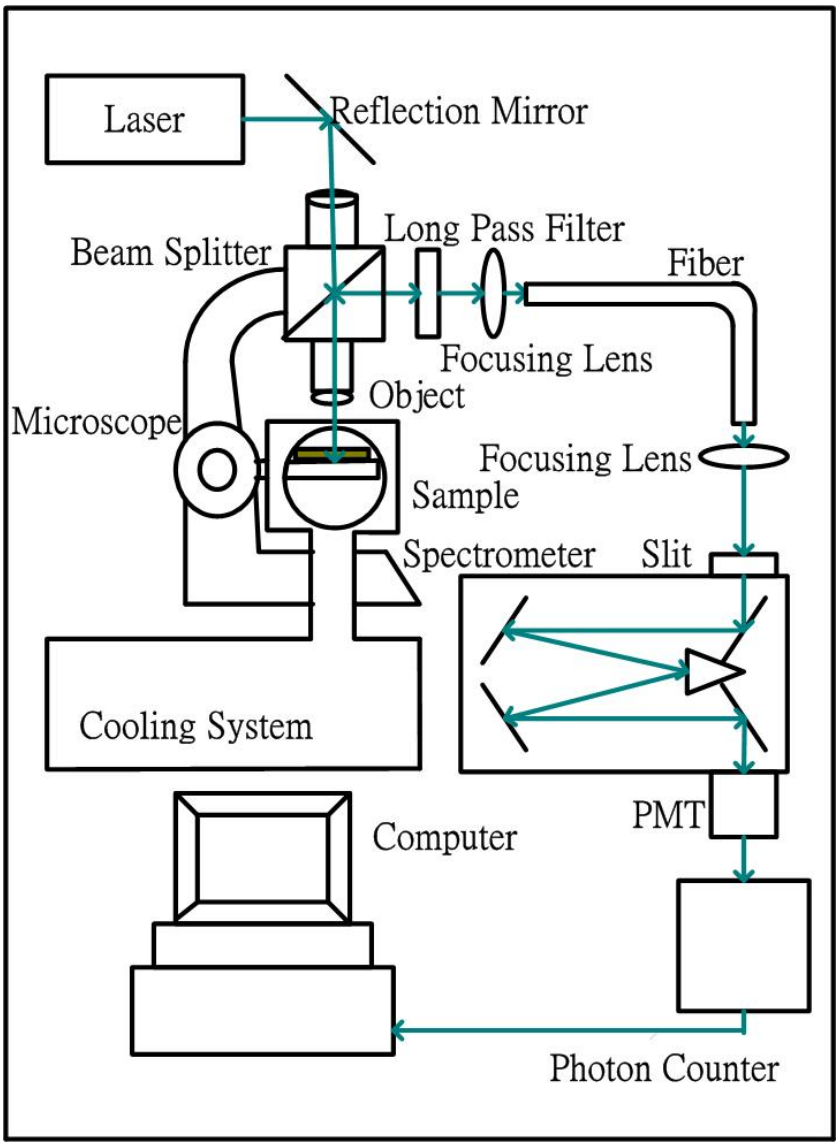

Fig. 3-3 Schematics of micro-PL set-up.

Chapter 4 Results and discussion

In this chapter, the morphology of disk-like self-organized GaN dots was investigated by AFM. The micro-PL spectroscopy was used to investigate the size dependent quantum confinement effect. Temperature-dependent PL spectra were analyzed to obtain the variation of emission peak energy on temperature. Exciton bound to the defect state in the dots and exciton thermalization from confined well states into the defect state of AlGaN layer were used to explain the temperature dependent PL results.

4.1 Morphology and size of GaN dots

Self-organized GaN dots were grown on $Al_{0.11}Ga_{0.89}N$ buffer layer using MOCVD. Fig. 4-1 (a) is a 2 μm x 2 μm AFM plane view image of the $Al_{0.11}Ga_{0.89}N$ buffer layer. The average roughness of the $Al_{0.11}Ga_{0.89}N$ buffer layer was approximately 0.25 nm, indicating that the surface of the $Al_{0.11}Ga_{0.89}N$ buffer layer is flat. Fig. 4-1 (b) to (h) show the 5 μm x 5 μm AFM plane-view images of the GaN samples grown on $Al_{0.11}Ga_{0.89}N$ buffer layers with different GaN coverage. The GaN coverage was estimated from the TMGa flow rate. For GaN coverage of 1.8 and 5.5MLs, no island formation was observed. As the GaN coverage was increased above 7.3MLs, self-assembled GaN dots was observed. This is a typical characteristic of the Stranski-Krastanow (S-K) growth mode which is a growth mode starts from a two-dimensional layer and then three-dimensional islands are formed after some critical thickness is reached [20].

Fig. 4-2 (a) to (c) illustrate the three-dimensional AFM images of single GaN dot. We found that the average lateral diameter is far greater than the height with the aspect

ratio (height/diameter) ranging from $\frac{1}{13}$ to $\frac{1}{50}$. The shape of GaN dot is disk-like and is different from that of previous reports [28-38]. Moreover, there are two kinds of shapes, symmetric and irregular types. For symmetric type, lens-like and ellipse-like GaN QD are shown in Fig.4-2 (a) and (b), respectively. The irregular type is shown in Fig.4-2 (c). The height profiles across the lens-like and ellipse-like QD are shown in Fig.4-2 (d) and (e), respectively. From the profile of the single ellipse-like dot, we find that this type of QD is composed of two dots. Most GaN QDs are lens-like. Furthermore, with an increasing GaN coverage, the number of irregular dot increases.

Fig. 4-3 illustrates the height distribution of GaN dots with different coverage. The solid lines are guide to the eyes. We found that the average height was about 5.7 to 8.2 nm and the standard deviation was about 2.1 to 2.8 nm. The dot size increases with the increasing GaN coverage. Linear dependence of the average height and width on the GaN coverage is shown in Fig. 4-4. The average dot size is about 6.6, 7.1, 8.2 nm in height and 190, 200, 215 nm in diameter for the GaN coverage of 9.1, 10.9, 13.6MLs, respectively. The estimated dot density is about $9.1\text{x}10^8$, $1.1\text{x}10^9$, $7.2\text{x}10^8/\text{cm}^2$ for the GaN coverage of 9.1, 10.9, 13.6MLs, respectively.

Fig.4-5 shows the dependence of the dot density on the GaN coverage. The solid curve is a theoretical fit by using equation $\rho = \rho_0(\Theta - \Theta_c)^\alpha$ proposed by D. Leonard et al., where ρ is islands density, Θ is estimated GaN coverage, and ρ_0 , Θc , and α are fitting parameters [42]. This model is applied to the quantum dots grown by SK mode. From the exploration of the solid curve to the x-axis, the thickness of wetting layer of 7.2MLs (1.8 nm) is obtained. For the GaN coverage exceeds 14MLs, the experiment data is beyond the solid curve. It is attributed to the coalescence of dots which leads to the decrease in dot density [32].

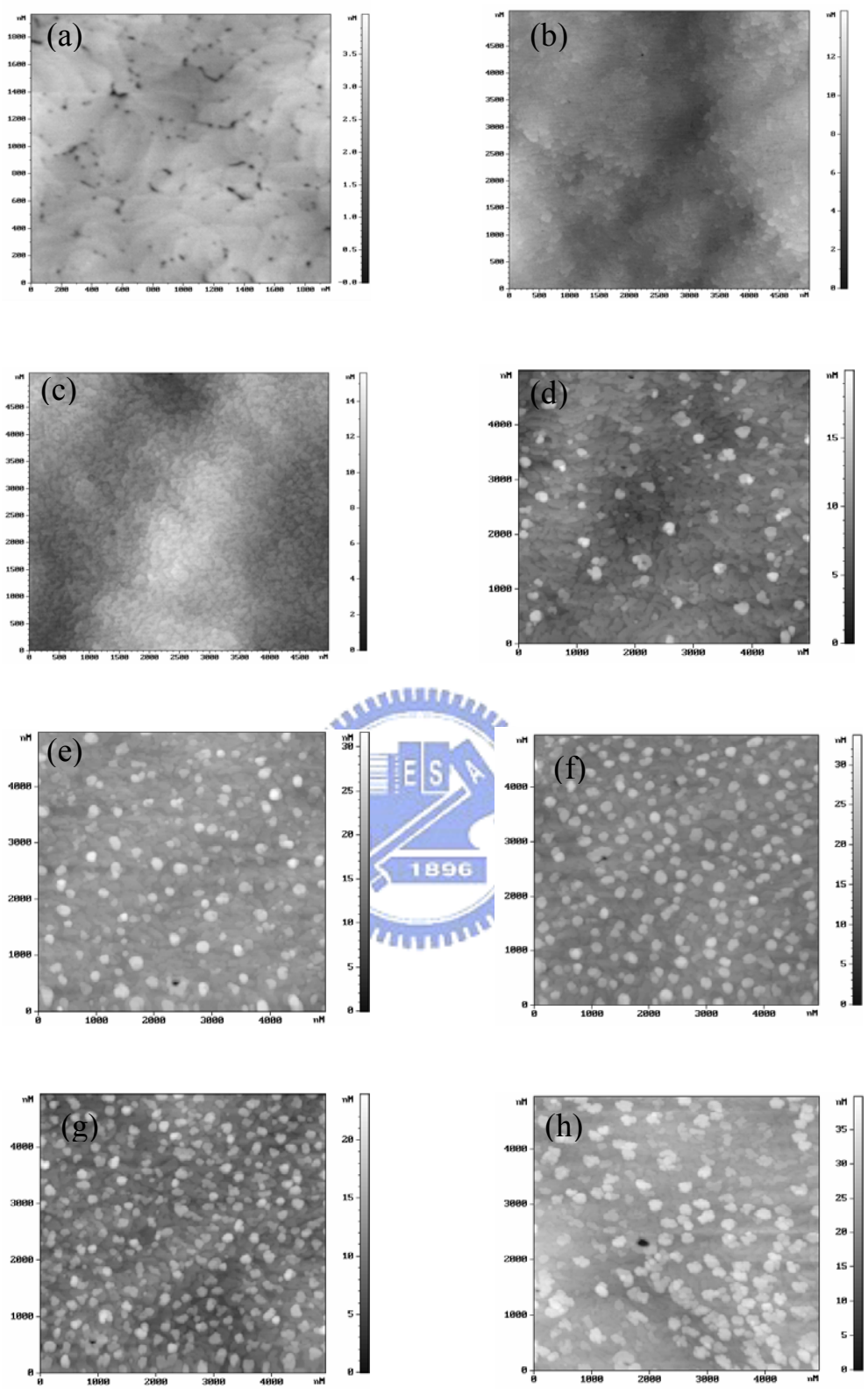

Fig. 4-1: The plane view image of a 2μm × 2μm AFM scan on $Al_{0.11}Ga_{0.89}N$ buffer layer (a), 5μm × 5μm images of the GaN samples grown on $Al_{0.11}Ga_{0.89}N$ buffer layers with different GaN coverage of (b) 1.8, (c) 5.5, (d) 7.3, (e) 8.2, (f) 9.1, (g) 10.9, and (h) 13.6 MLs.

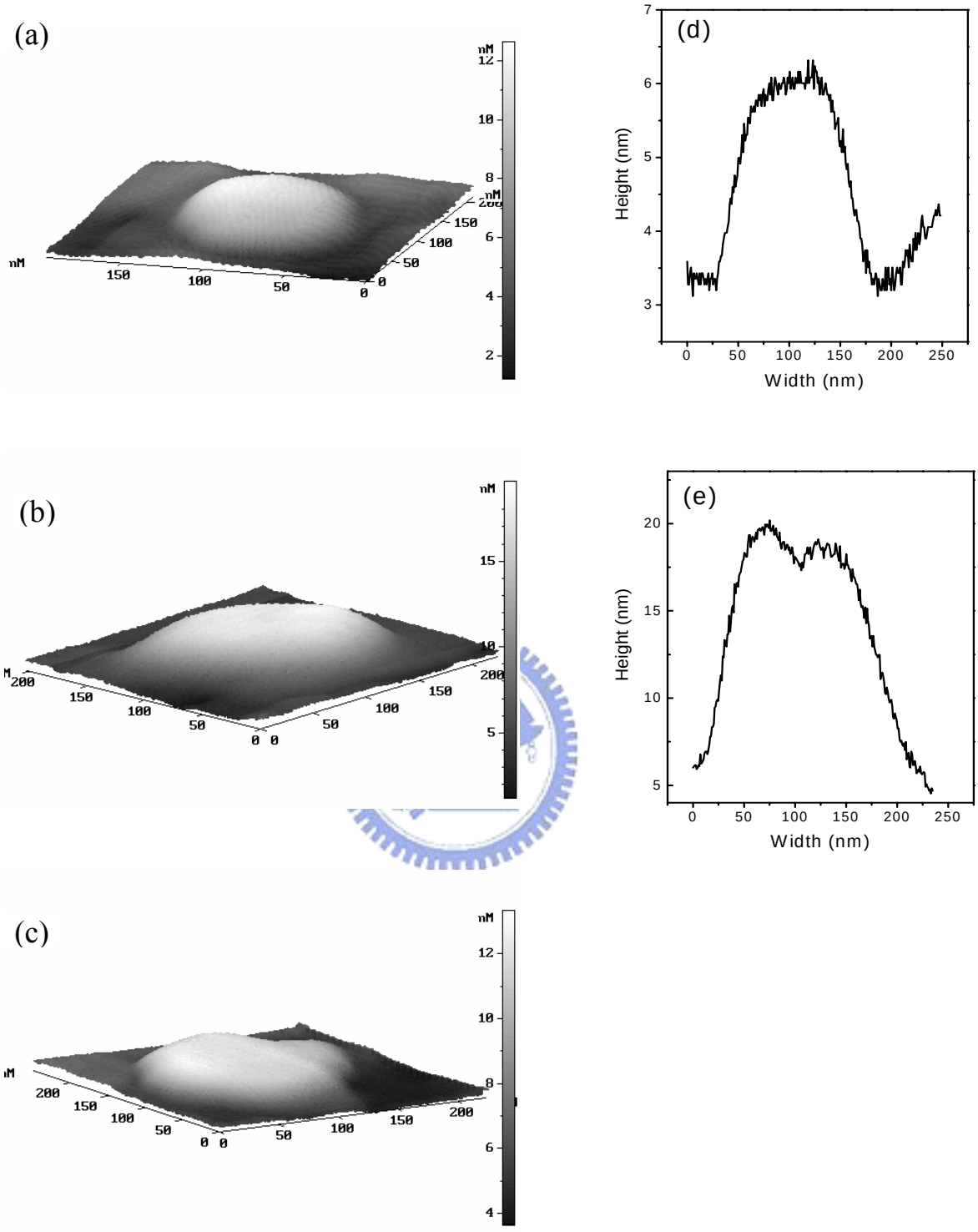

Fig. 4-2. Three dimensional AFM images of single GaN dot of (a) flat-lens, (b) flat-ellipse, (c) irregular,. (d) and (e) are the lateral profiles of (a) and (b), respectively.

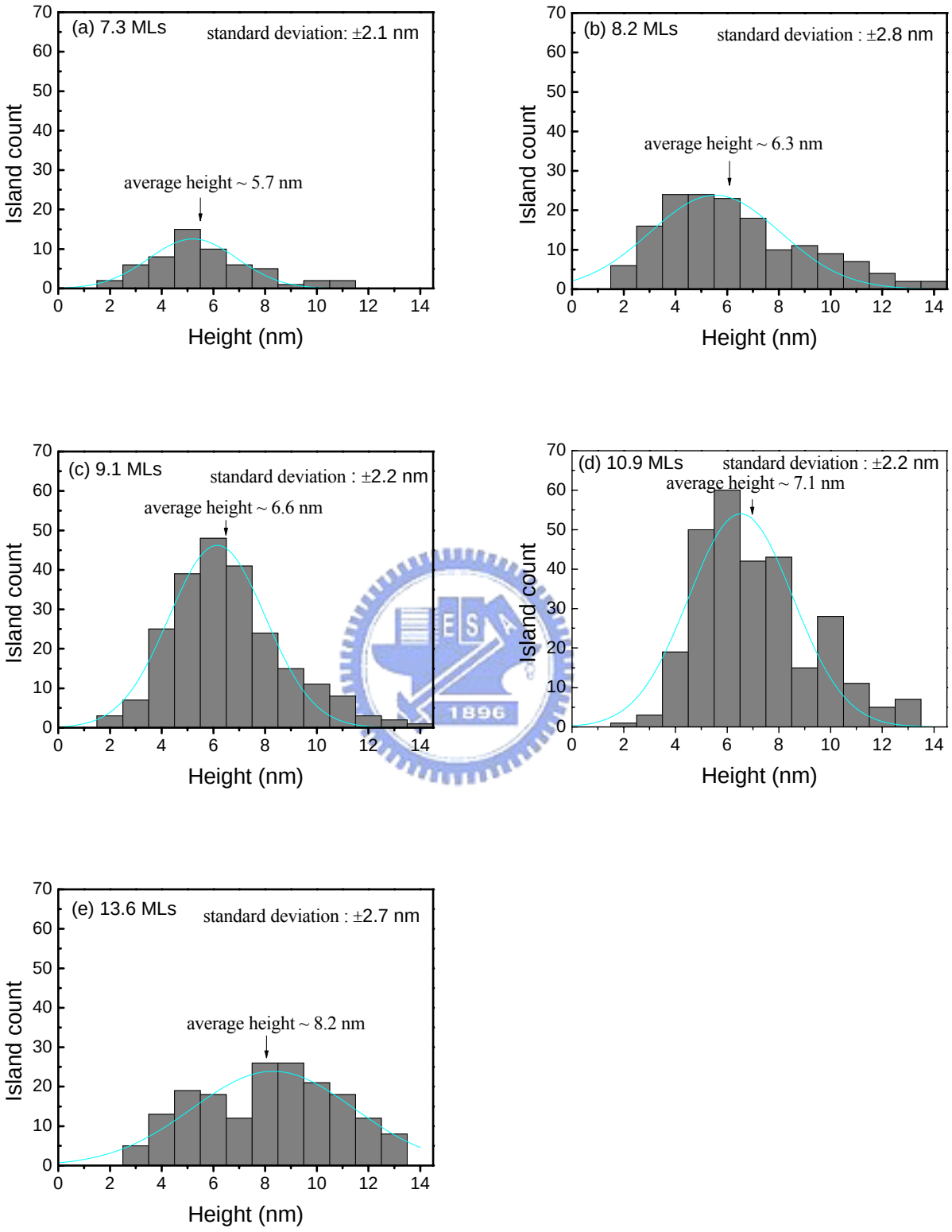

Fig. 4-3 Histograms of dot height distribution with different GaN coverage of (a) 7.3, (b) 8.2, (c) 9.1, (d) 10.9, and (e) 13.6 MLs. The solid lines are guide to the eyes.

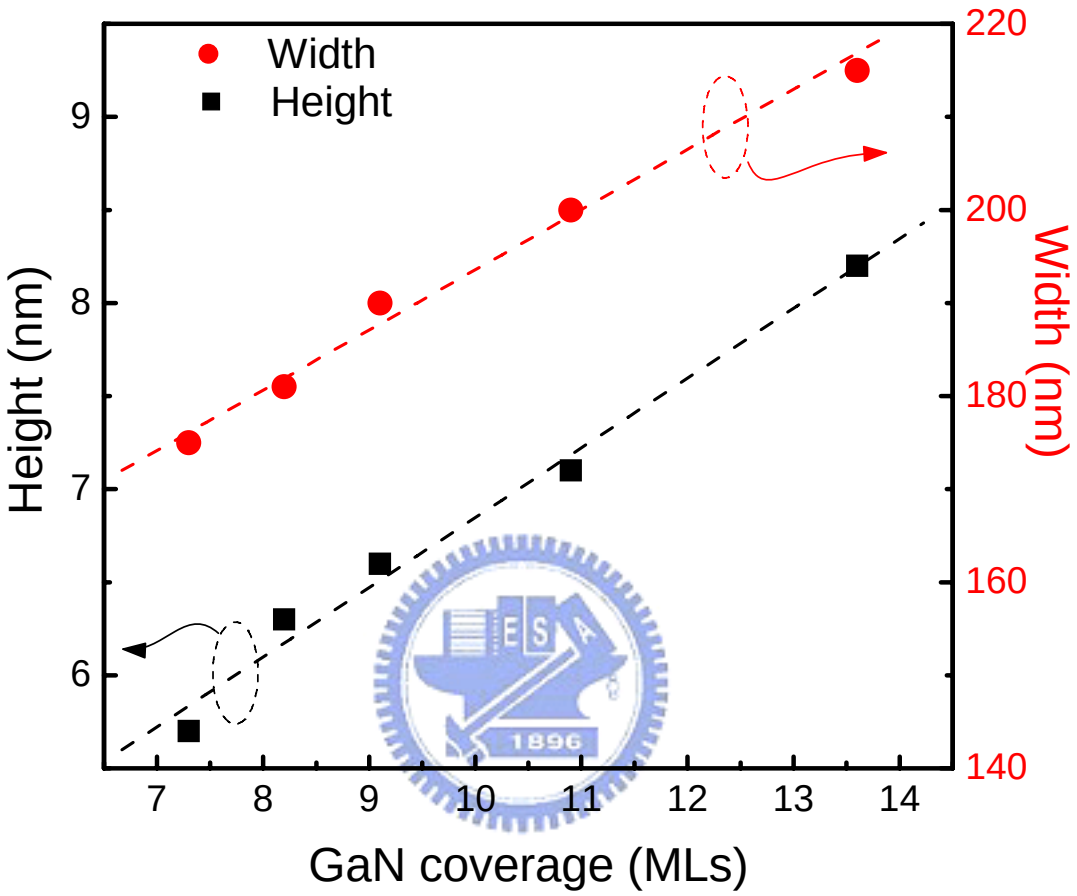

Fig. 4-4: Dependence of average height and width on the GaN coverage. The dashed lines are guides to eyes.

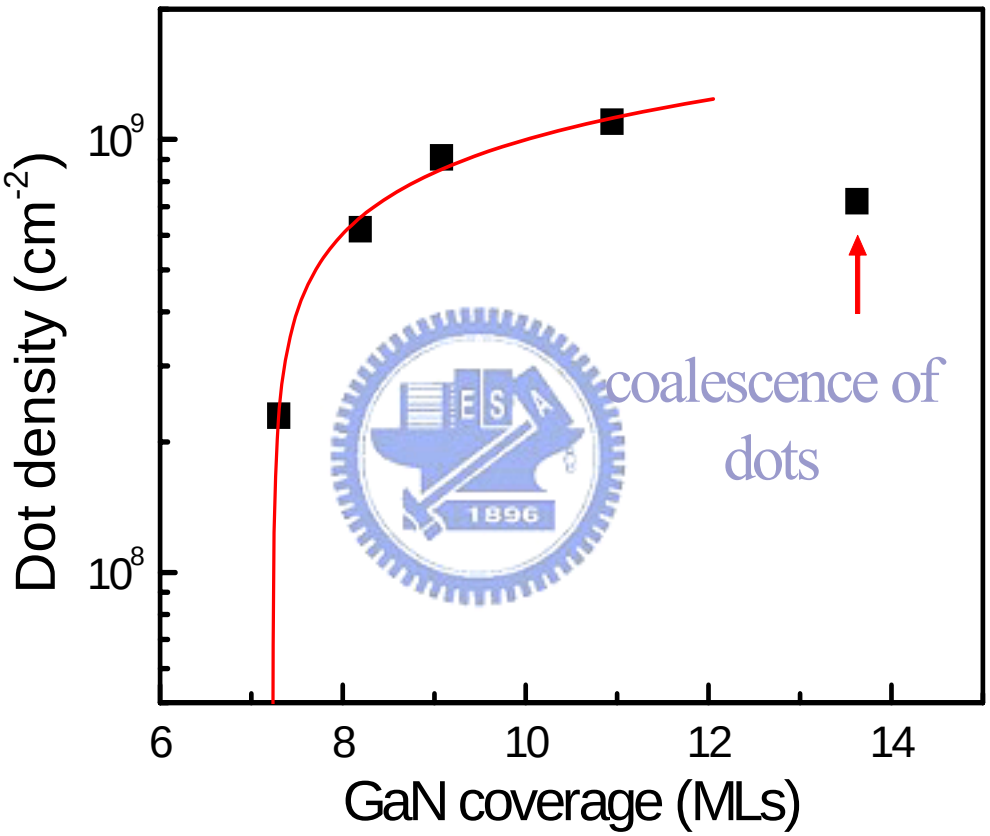

Fig. 4-5: Dependence of islands density on the GaN coverage. The solid line is a theoretical fit.

4.2 Size dependent micro-photoluminescence spectra

The PL spectra of the self-organized disk-like GaN dots with different coverage at 10 K were shown in Fig. 4-6. The 10 K PL spectra of GaN and $Al_{0.11}Ga_{0.89}N$ epilayers were shown as reference in Fig. 4-6 (a) and (b), respectively. The peak emission situated at 3.48 eV is ascribed to the near band edge emission (NBE) of GaN [43]. In Fig. 4-6 (b), the PL peak located at 3.651 eV corresponds to the NBE emission of the $Al_xGa_{1-x}N$ epilayer, whose Al composition of the 11% was confirmed by x-ray diffraction analysis of the epitaxial layers [43]. The PL peak energy located at 3.594 eV, which is 57 meV lower than NBE, was not a phonon replica because the longitudinal optical phonon energy is 94 meV for $Al_{0.11}Ga_{0.89}N$. It was suggested to be a defect-related emission from the $Al_{0.11}Ga_{0.89}N$ epilayer in Fig.4-6 (b) or $Al_{0.11}Ga_{0.89}N$ buffer and capping layer in Fig. 4-6 (c) to (e). In Fig.4-6, the PL intensity is normalized according to the intensity of NBE from the $Al_{0.11}Ga_{0.89}N$ buffer layer or capping layer.

Figs. 4-6(c) to (e) show the PL spectra of the GaN QDs grown on $Al_{0.11}Ga_{0.89}N$ buffer layers with different GaN coverage. When GaN coverage is less than 8.2MLs, the dot density is too rare for the dot emission to be detected. In current study, the optical spectroscopy of GaN dots is confined to the samples of 9.1, 10.9, and 13.6MLs. All the samples for PL studies were capped with 30 nm $Al_{0.11}Ga_{0.89}N$ layer whose Al content was the same as the buffer layer (11%), as shown in Fig. 3-1 (b). The PL labeled as I_{QD} is attributed to the luminescence emitted from the GaN dots. Note that the peak positions of I_{NBE} from the $Al_{0.11}Ga_{0.89}N$ buffer layer and/or capping layer are roughly the same for all three GaN dots, indicating the aluminum composition fluctuation of AlGaN buffer layers and capping layers is negligible in these samples. Furthermore, no luminescence related to the wetting layer was observed in PL at 10 K or RT. The absence of the luminescence related to the wetting layer is most likely due to the fact that the carriers photogenerated in the wetting layer transfer to the adjacent GaN dots

and then recombine there [44].

The peak energy position and full width at half maximum (FWHM) of PL spectra at 10 K are summarized in Fig. 4-7. The PL peak position of the disk-like GaN dots grown under 9.1, 10.9, and 13.6MLs of GaN coverage situate at 3.546, 3.510, 3.487 eV at 10 K, respectively. The PL peak energy of GaN epilayer is 3.480 eV at 10 K for reference. We found that all of the GaN QD samples exhibited large blue-shifts in the PL spectra compared with GaN epilayer (from 36 to 62 meV at RT), even though the shape of QDs are disk-like. Ramvall et al. [45] calculated the energy shift of the electronic level to fit the experimental data of GaN quantum dots and showed that energy shift as large as 125.9 meV is possible for a quantum dot of 10 nm in diameter and 3.5 nm in height. To analyze the line width dependence of dot-related emission peak (I_{QD}) on the size distribution, PL peaks were fitted by Gaussian curve. All the peak energy and FWHM of PL peaks were derived from the fitting value. The red-shift in the energy with the increasing GaN coverage is attributed to the decrease in the quantum confinement energy as the dot size is increased. In order to further explain the blue-shift with reducing dot size in the PL spectra quantitatively, we consider an electron or a hole in a rectangular box for simplicity. Therefore, the confinement energy of the ground state is expressed as:

$$E = \frac{h^2}{8}\left(\frac{1}{m_x d_x^2} + \frac{1}{m_y d_y^2} + \frac{1}{m_z d_z^2}\right) \quad \text{..... (1).}$$

Where, d_x, d_y, and d_z denote the dimensions of the box and m_x, m_y, and m_z represent the effective mass of electron or hole in x, y, and z directions, respectively. For a disk-like dot, the in-plane sizes d_x and d_y are much larger than the height d_z = d. Therefore, equation (1) will be simplified as

$$E = \frac{h^2}{8m_{ez}d^2} + \frac{h^2}{8m_{hz}d^2} \quad \text{..... (2).}$$

Where, the electron effective mass m_{ez} equals 0.2 m_0, the hole effective mass m_{hz} equals 1.0 m_0, m_0 is the electron rest mass[33]. In Fig. 4-8, the solid curve is plotted by using equation (2). The triangular points represent the PL data. The horizontal bars are obtained from AFM measurements to represent the size fluctuation. We show that the experimental results fit in with this simplified model quantitatively.

In addition to an increasing confinement shift with decreasing physical size of the dots, an increased inhomogeneous broadening can be also observed. From Fig. 4-7, the FWHM of the PL peak from GaN dots range from 56 to 88 meV at 10 K. It was 11.6 meV for GaN epilayer. Compared with bulk GaN, the FWHM of dot is relatively larger which may originate from the dot size fluctuation. In order to illustrate that the larger FWHM of QD PL spectra is mainly induced by size fluctuation, we will calculate the size fluctuation induced FWHM. The method is demonstrated in Fig. 4-9, where the error bar of x-axis denotes the height inhomogeneity. Fig 4-10 shows the PL FWHM at 10 K and RT as well as the size fluctuation induced FWHM. From comparison, we find that the PL FWHM at RT is relatively larger than FWHM at 10 K and the size fluctuation induced FWHM, indicating the carrier-phonon scattering increases with increasing temperature. In addition, the FWHM at 10 K is close to the size fluctuation induced FWHM. Therefore, we can confirm that the PL FWHM of I_{QD} is derived from size inhomogeneity and the increasing of the FWHM with the decreasing size is attributed to the increasing of the size fluctuation.

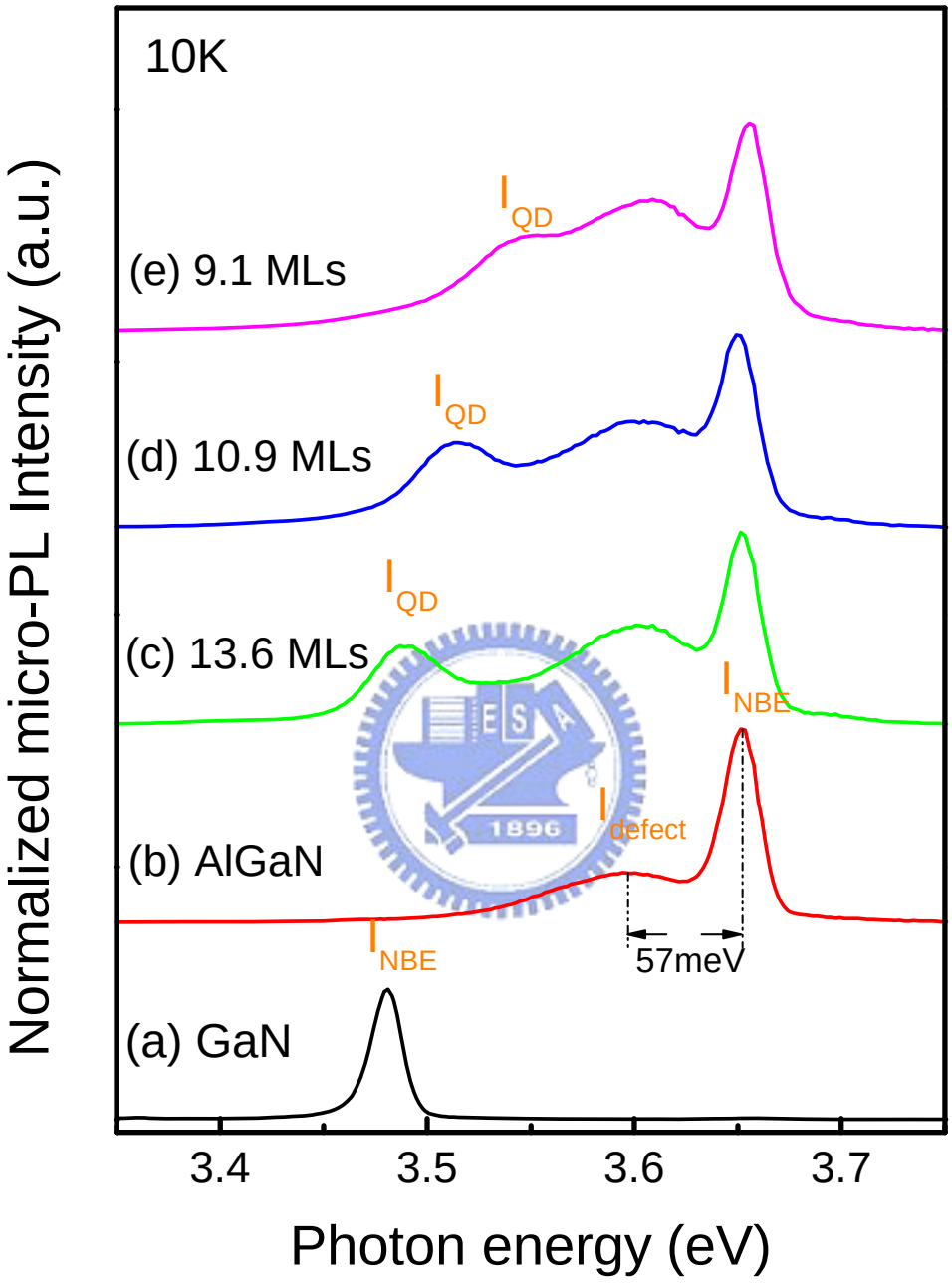

Fig. 4-6 Normalized μ-PL spectra at 10 K of (a) GaN epilayer, (b) $Al_{0.11}Ga_{0.89}N$ epilayer, and the GaN samples grown on $Al_{0.11}Ga_{0.89}N$ buffer layers with different GaN coverage of (c) 9.1 MLs, (d) 10.9 MLs, and (e) 13.6 MLs.

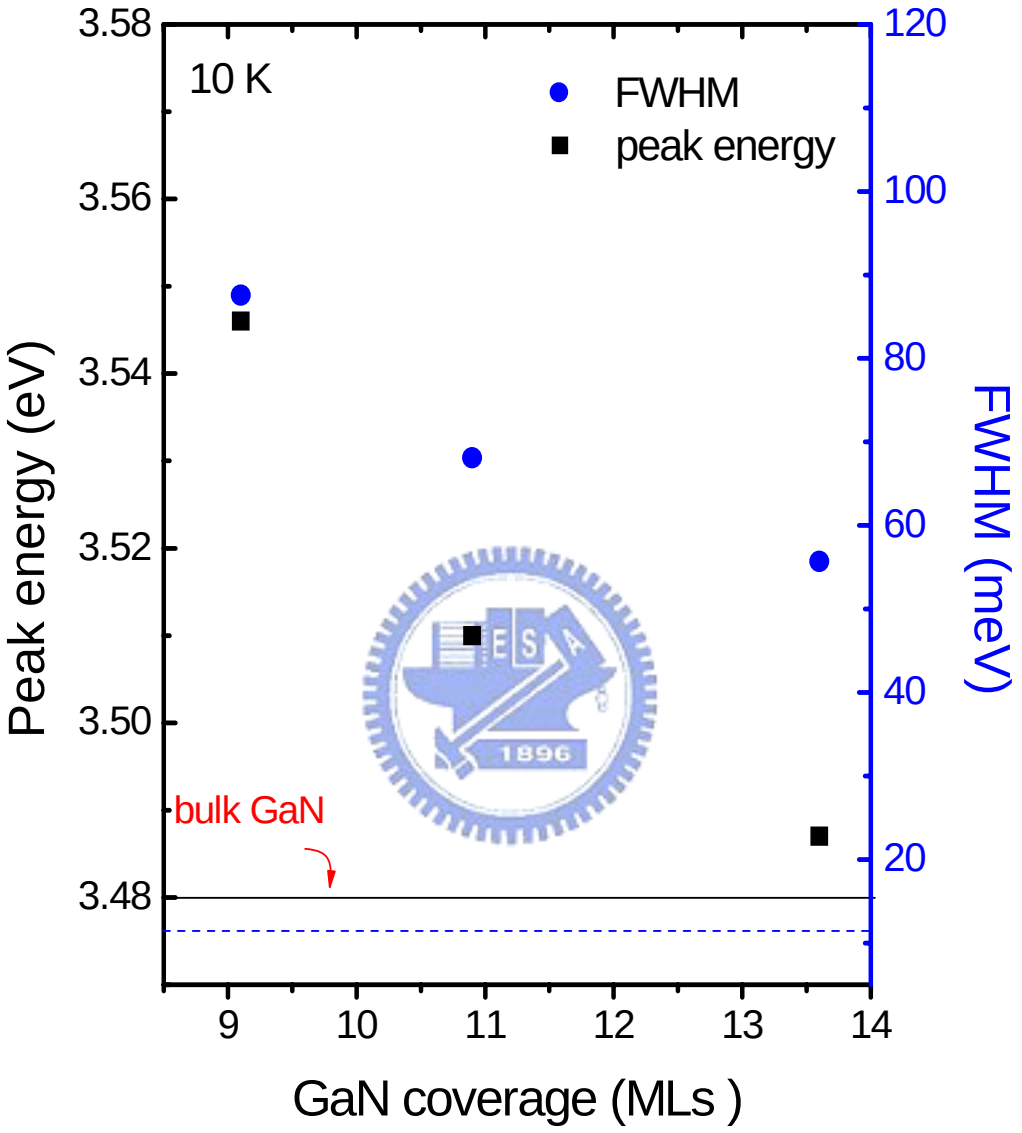

Fig. 4-7 The peak energy and FWHM of μ-PL spectra of the GaN samples grown on $Al_{0.11}Ga_{0.89}N$ buffer layers with different GaN coverage at 10 K.

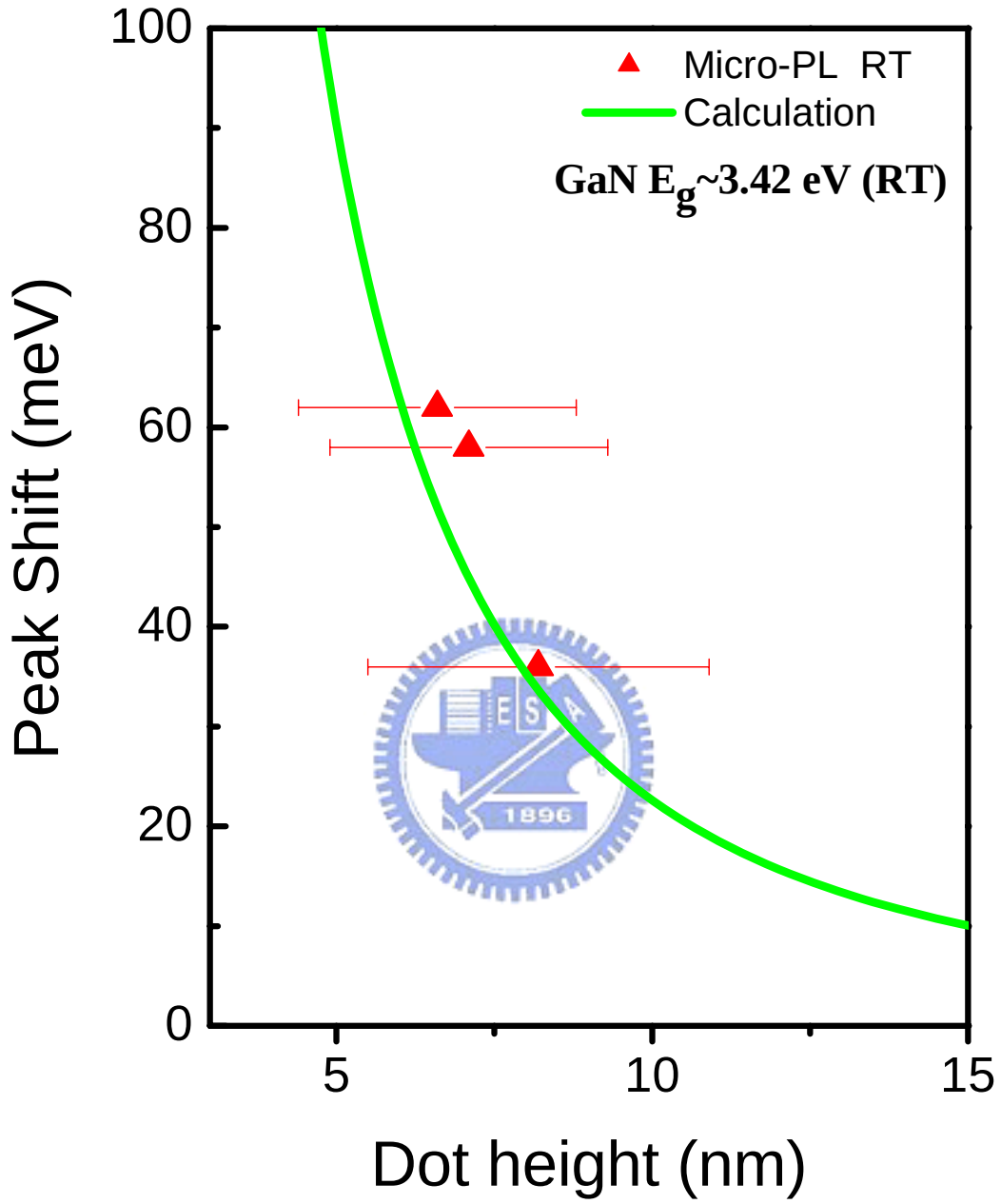

Fig. 4-8 Comparison with the PL experimental data and calculation derived from the disk-like rectangular box model.

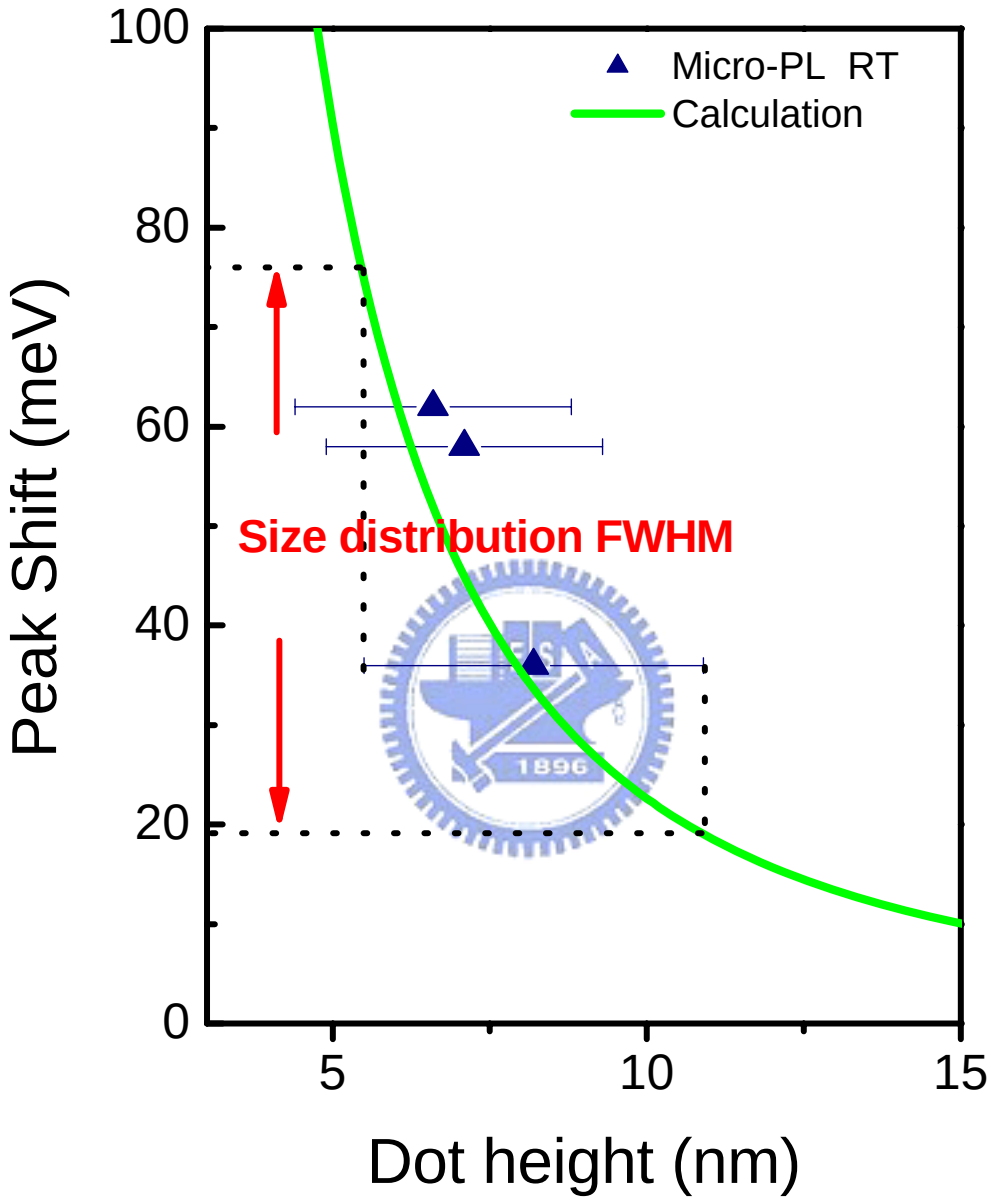

Fig. 4-9 Demonstration of size distribution FWHM.

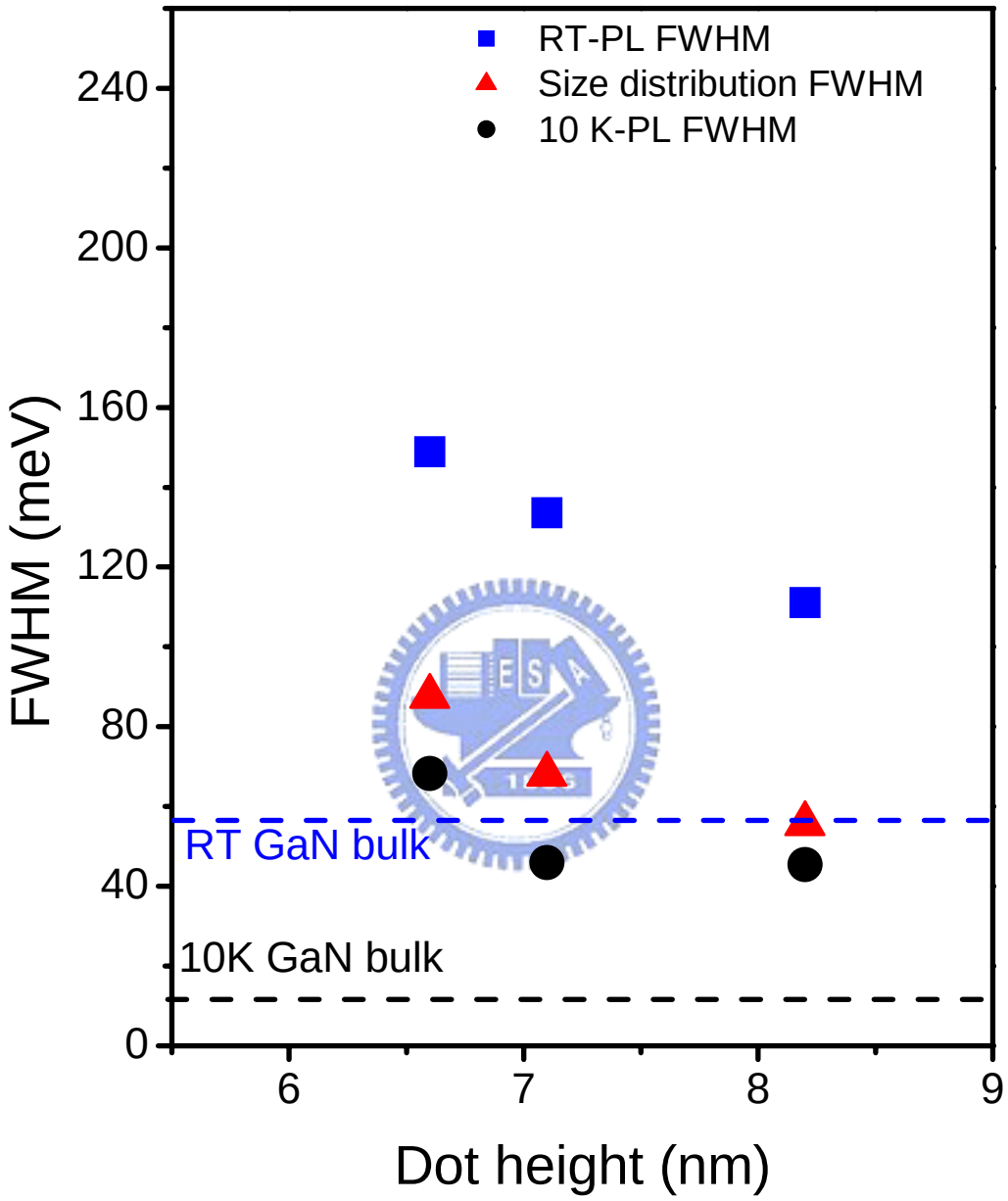

Fig. 4-10 Comparison with FWHM of PL spectra and size distribution.

4.3 Temperature dependent micro-PL spectra

4.3.1 Temperature variation of PL peak energy

Figs. 4-11, 4-12, 4-13 show the temperature dependent PL spectra of the GaN dots with height of 6.6, 7.1, 8.2 nm in the temperature range from 10 K to room temperature (RT), respectively. There are three important issues must be addressed for temperature dependent PL temperature: (i) temperature-dependent energy shifts, (ii) the line broadening with temperature, (iii) activation energy, which characterizes the temperature stability of the material system. Fig. 4-14 presents the temperature dependent PL peak energy for the samples of different dot height. PL peak energy as a function of temperature for the GaN epilayer is shown as reference. The solid line presents the fitting of Varshni's law for GaN dots. The broken line is the temperature dependent band gap of GaN epilayer shifted to a higher energy for comparison with the solid line of QD. Varshni's equation [46], as shown below, was employed to fit the experimental data.

$$E(T) = E(0) - \frac{\alpha \mathrm{T}^2}{[\mathrm{T} + \beta]}$$

where $E_g(T)$ and $E_g(0)$ are the band gap at temperatures T and 0 K. α and β are fitting parameters that are characteristic of a given material. The variation of the peak position with temperature can be attributed to the effect of dilation of lattice and electron-lattice interaction. Theoretical treatments show that these effects should follow the Varshni's relation. In our results, the temperature dependence of peak energy obeys the Varshni's law in the high temperature regime nicely. However, it is a striking feature that PL peak energy exhibits initially a blue-shift with increasing temperature and then followed by a red-shift. Such an energy shift with increasing temperature has also been observed in other QDs system [47]. This is the typical characteristics of the exciton localization. The localization energy of 5 meV for GaN epilayer is ascribed to the

donor-bound exciton [48]. However, the degree of exciton localization increases with dot size, which varying from 6 to 28 meV. We believe that the exciton can be bound to the certain state in the dots. When the temperature was raised, the bound exciton was thermalized to free exciton, and hence the blueshift of PL peak energy was observed.

Another feature is temperature variation of PL peak energy of dots follows the behavior of GaN epilayer, as shown in Fig. 4-14. In our disk-like QDs, the initial narrowing in FWHM then broadening with the increasing temperature, which is a signature of the Stranski-Krastanow dots [49, 50], was not observed, as shown in Fig. 4-15. Therefore, we believe that the exciton transfer between QDs is impossible in our disk-like dot system. Fig.4-16 illustrates the band diagram at low T. We suggest that there exist the defect state in the dots which localize the exciton at low T. The exciton were thermalized from the defect bound state to the QD ground state with increasing T.

4.3.2 Temperature variation of PL integrated intensity

In order to identify the mechanism of the PL quenching, the temperature dependence of the PL integrated intensity of GaN dots is investigated (as displayed in Fig. 4-17). These data can be theoretically fitted using the Arrhenius equation. The solid line represents the fitting of Arrhenius equation, as shown below.

$$I(T) = \frac{I(0)}{\left[1 + C_1 \exp(-\frac{E_{a1}}{kT}) + C_2 \exp(-\frac{E_{a2}}{kT})\right]}$$

Where, I(T) and I(0) are the respective integrated intensity at temperatures T and 0 K. C_1 and C_2 are fitting parameters. E_{a1} and E_{a2} are the thermal activation energies dominated at the low and high temperature regime, respectively. An activation energy of 33 meV for GaN epilayer is ascribed to the binding energy of exciton [51]. However, we find that both activation energies also have a size-dependent behavior for disk-like dots. It is found that the larger dot size has the higher activation energy. The activation energies for E_{a1} are 7±2, 14±1, and 30±2 meV for 6.6, 7.1, and 8.2 nm dots, respectively.

Those values are close to the localization energy at low T of Fig. 4-14. The activation energies for E_{a2} are 43±4, 70±13, and 106±13 meV for the 6.6, 7.1, and 8.2 nm dots, respectively. In our samples, the energy differences (E_b) between the PL peak energy and $Al_{0.11}Ga_{0.89}N$ barrier band gap are 114, 131, and 173 meV at 100 K for 6.6, 7.1, and 8.2 nm dots, respectively. We can clearly understand that the exciton cannot be thermalized to the barriers because the difference between the PL peak energy and the band gap of barriers under investigation is significantly larger than the obtained activation energy (E_{a2}). However, we find that the energy differences between the defect state of $Al_{0.11}Ga_{0.89}N$ layers and the QD exciton transition energy is close to the activation energy (E_{a2}). Fig.4-18 illustrates the band diagram at high T. We suggest that the exciton escapes from confined well states into the defect state of $Al_{0.11}Ga_{0.89}N$ layers.

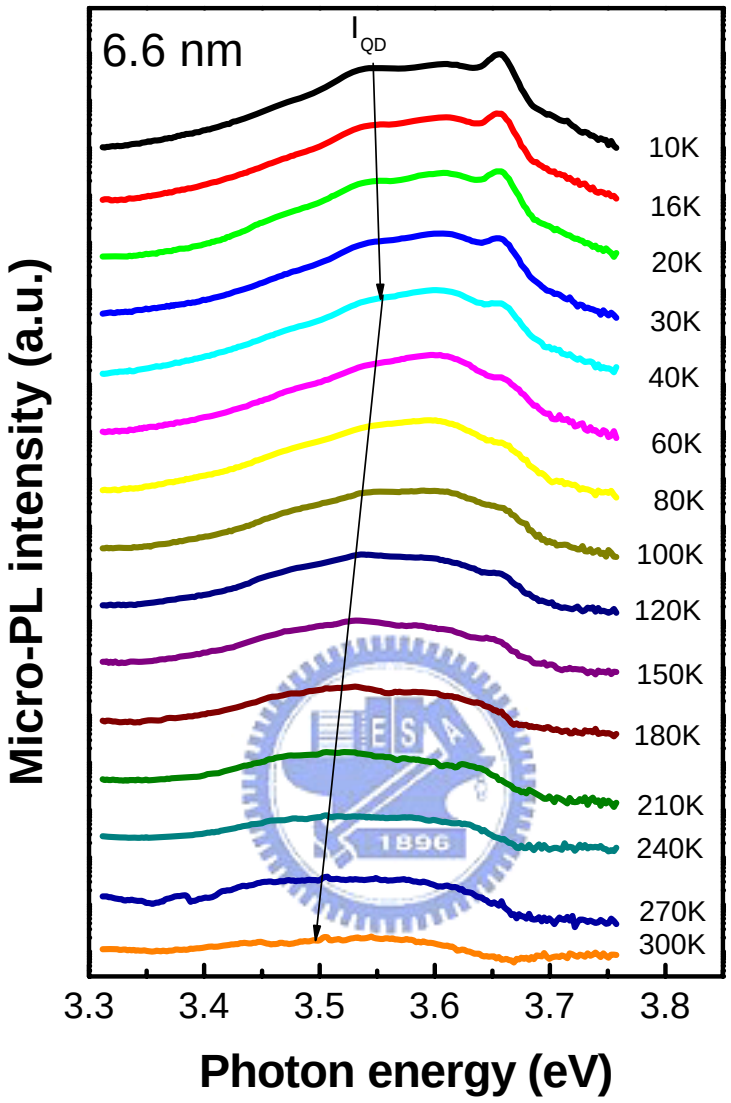

Fig. 4-11 Temperature dependent PL spectra of GaN dots with coverage of 9.1 MLs. The 6.6 nm is an average height for GaN dots.

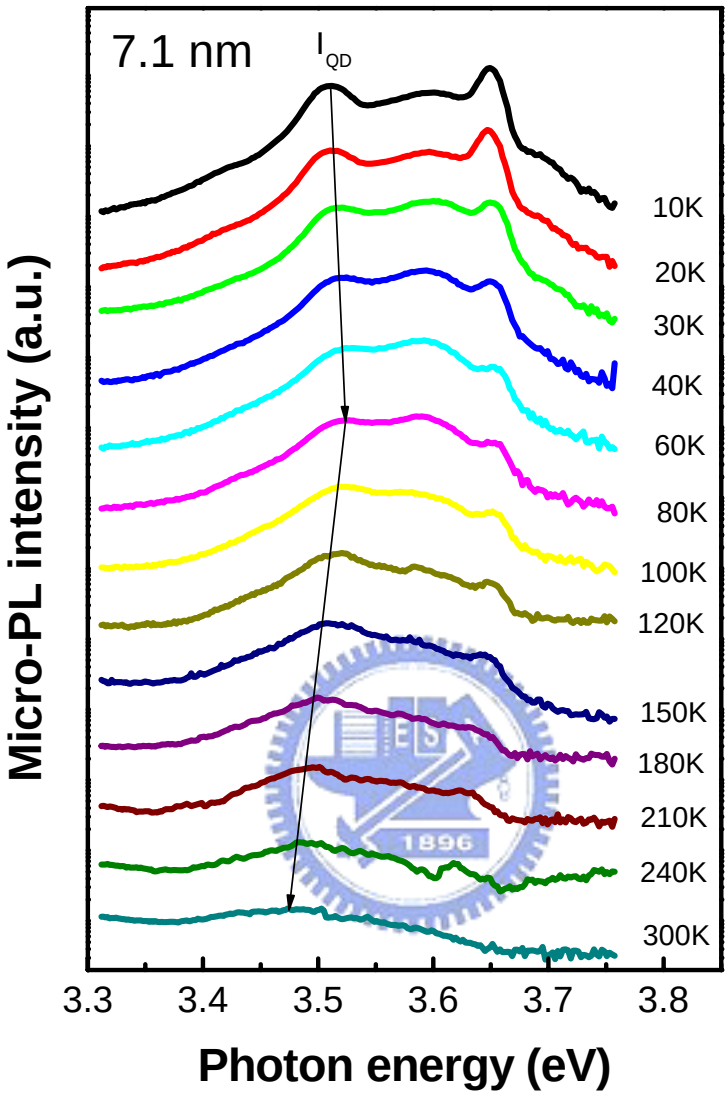

Fig. 4-12 Temperature dependent PL spectra of GaN dots with coverage of 10.9 MLs. The 7.1 nm is an average height for GaN dots.

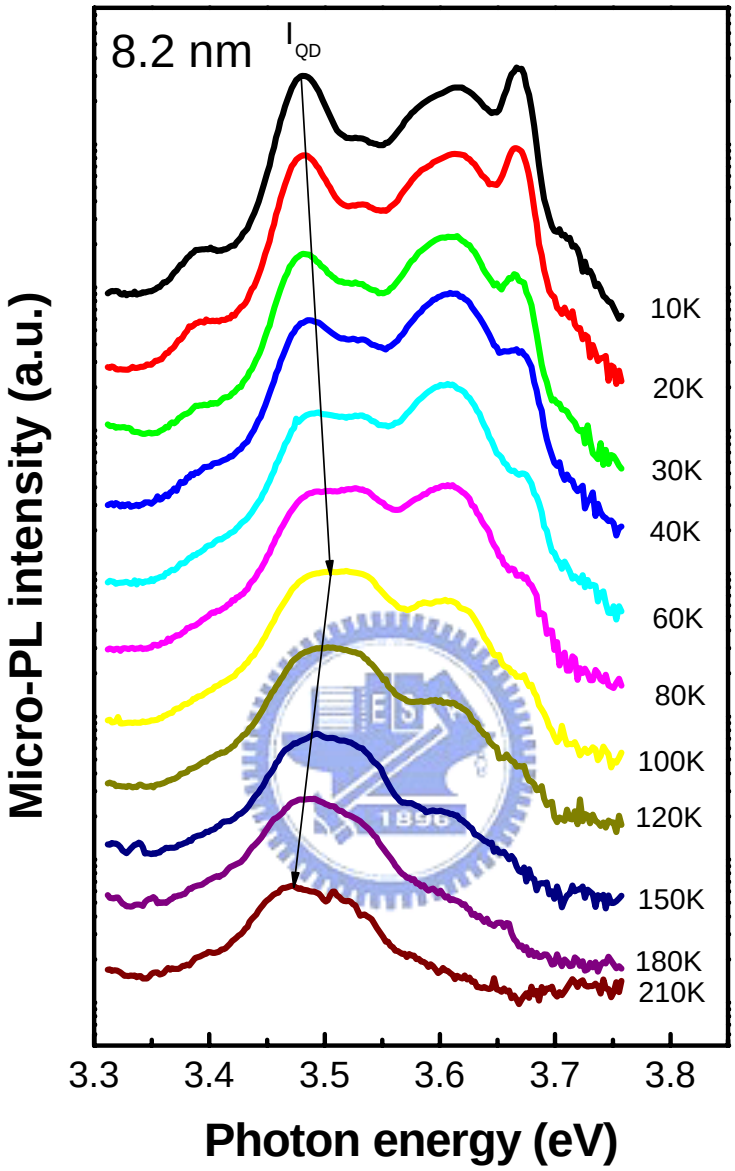

Fig. 4-13 Temperature dependent PL spectra of GaN dots with coverage of 13.6 MLs. The average height of GaN dots is 8.2 nm.

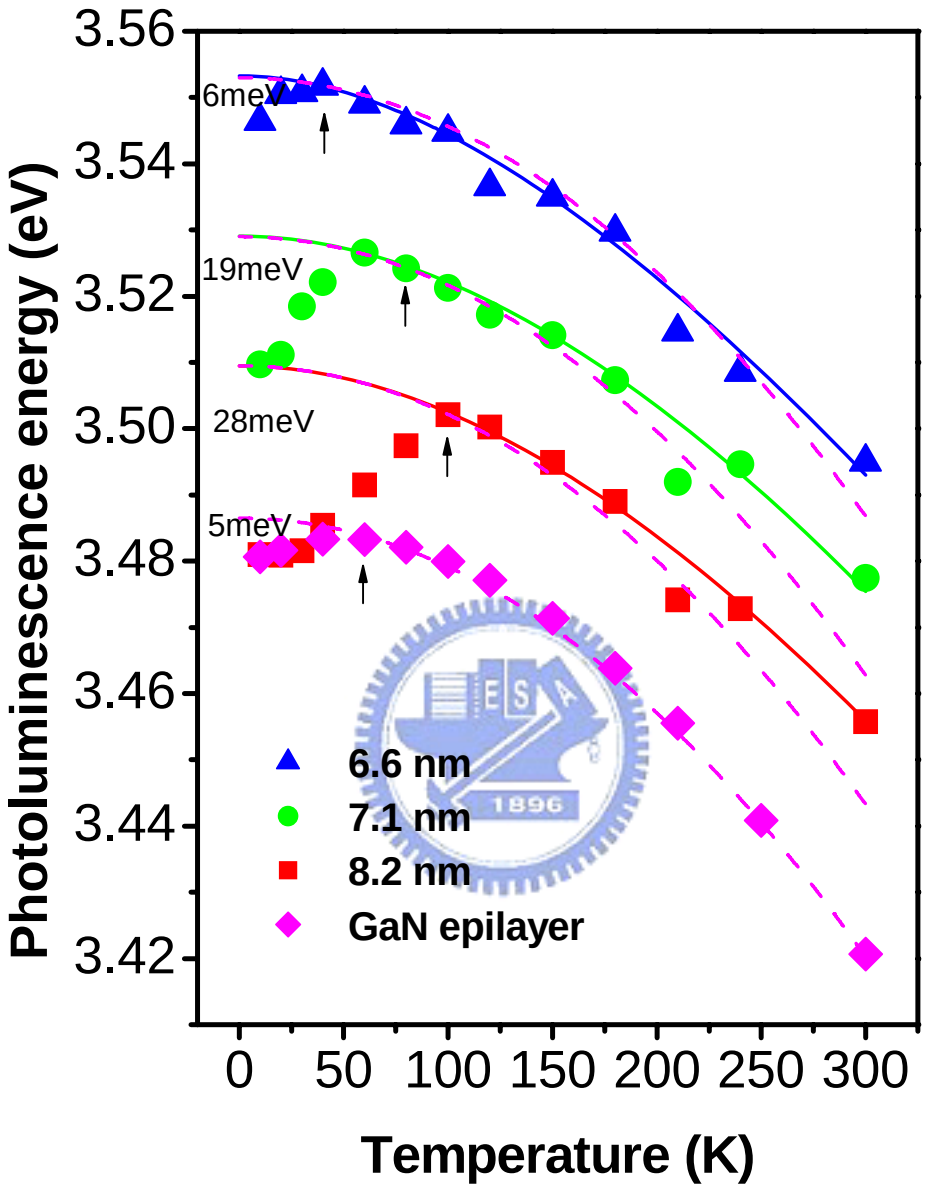

Fig. 4-14 PL peak energy as a function of temperature for the 6.6-nm, 7.1-nm, 8.2-nm GaN dot and the GaN epilayer. The broken line is the band gap of GaN shifted to a higher energy for comparison with the data. The solid line is a fit to the data by Varshni's equation.

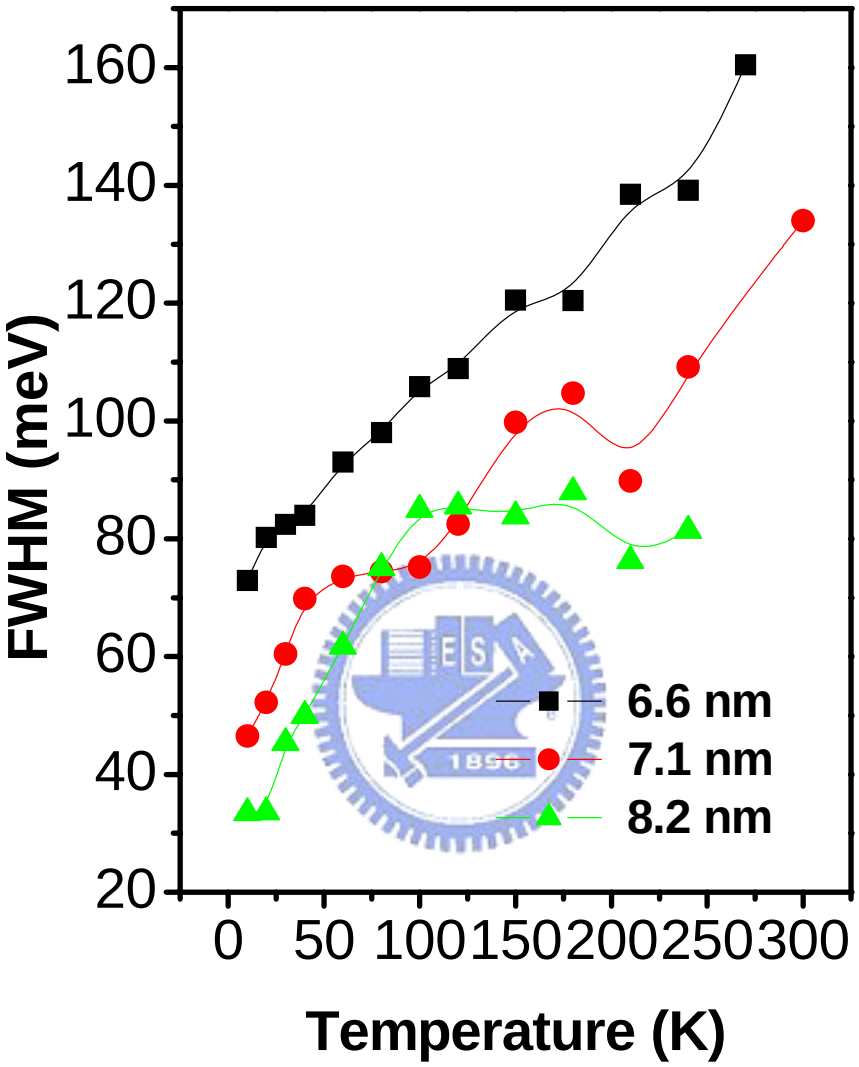

Fig. 4-15 FWHM of PL peak as a function of temperature for the 6.6-nm, 7.1-nm, and 8.2-nm samples. The solid lines are guide to the eyes.

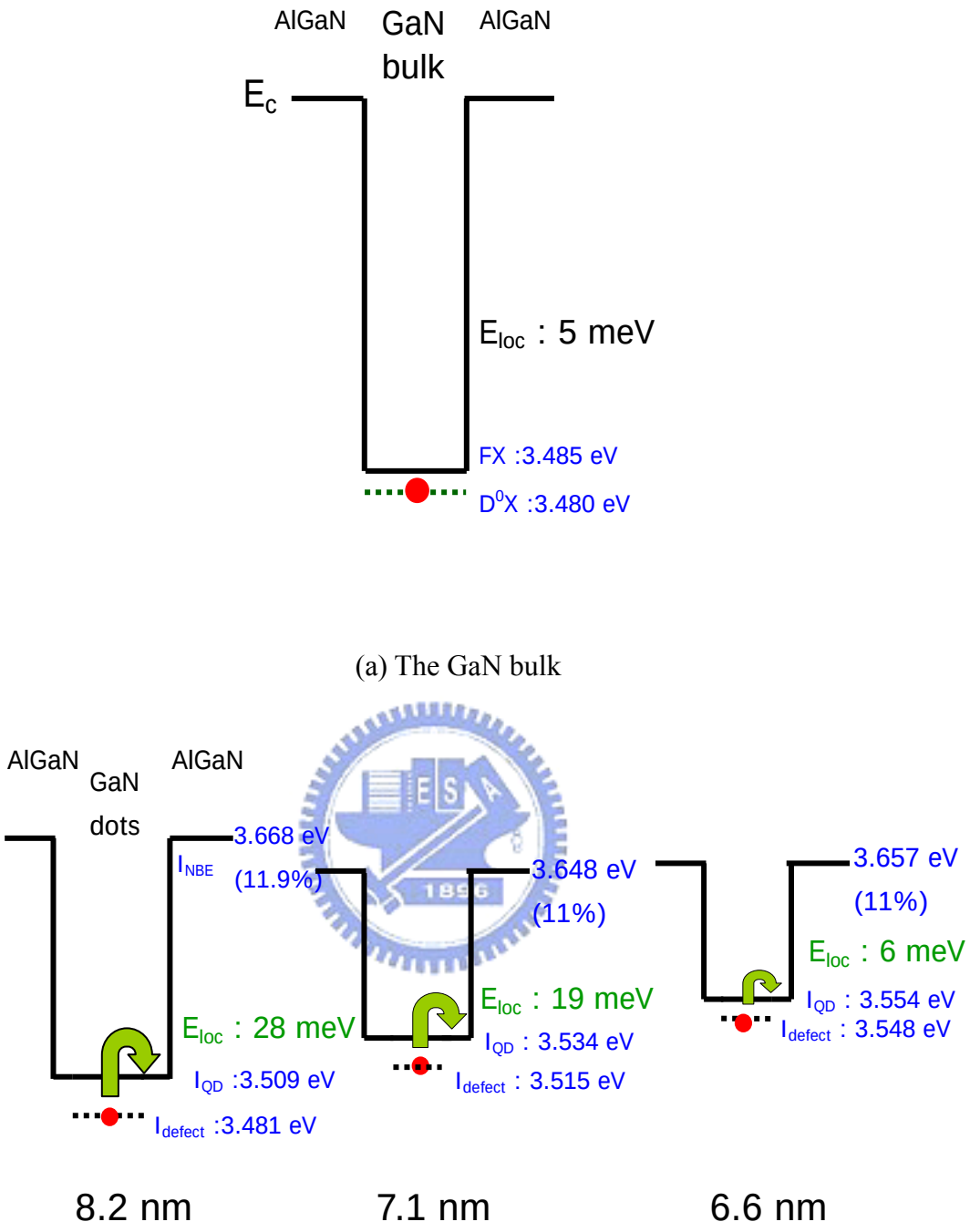

(a) The GaN bulk

(b) The disk-like GaN dots

Fig. 4-16 Schematic band diagrams near 10 K for (a) GaN bulk, (b) the disk-like GaN dots with height of 6.6, 7.1, and 8.2 nm.

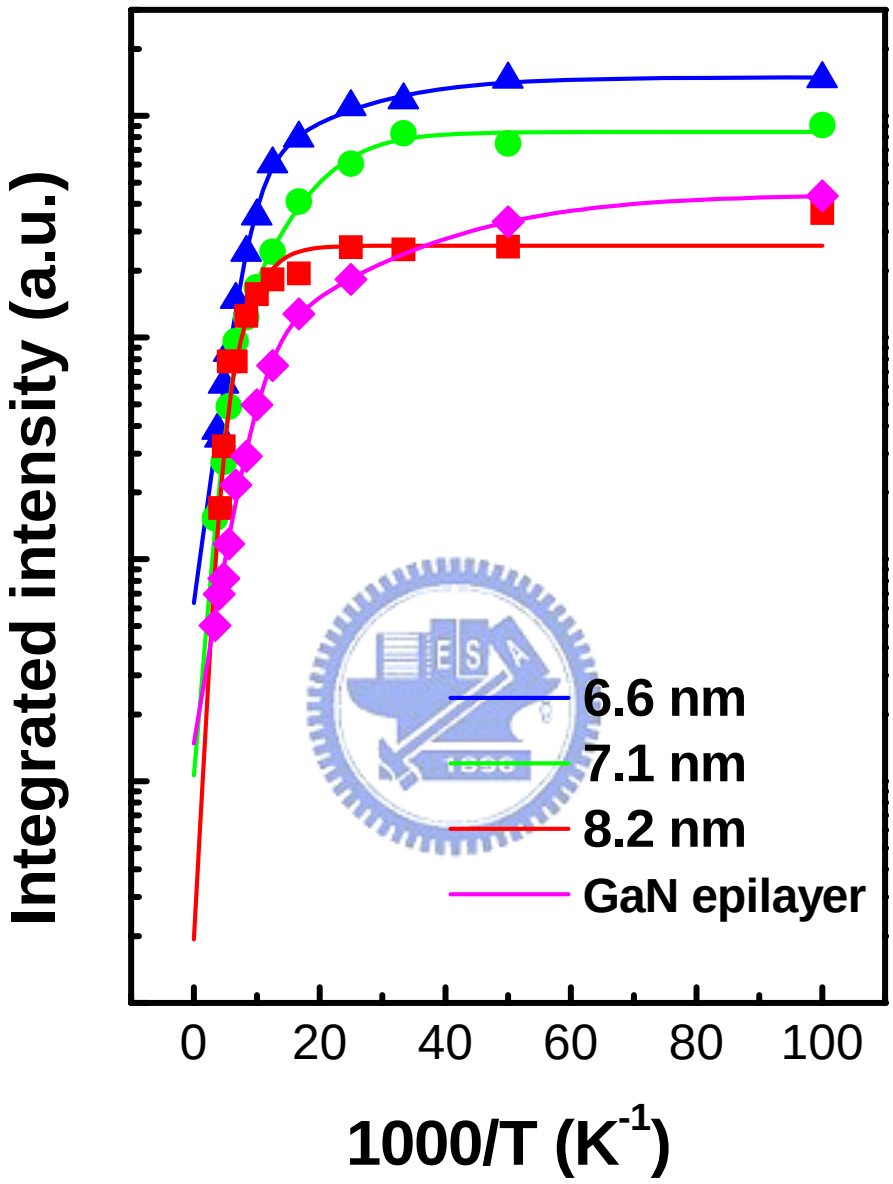

Fig. 4-17 PL integrated intensity as a function of temperature for the dot height of 6.6 nm, 7.1 nm, 8.2 nm and the GaN epilayer. The solid lines represent the fitting of Arrhenius equation.

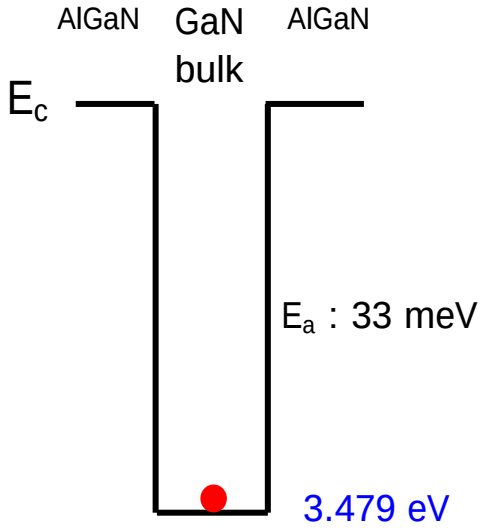

(a) The GaN bulk

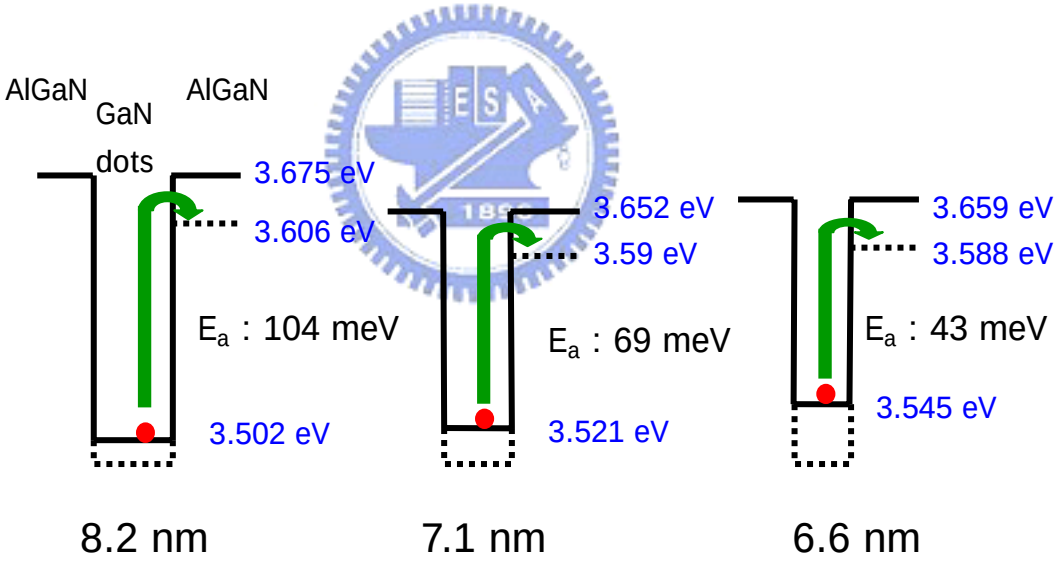

(b) The disk-like GaN dots

Fig. 4-18 Schematic band diagrams at high temperature for (a) GaN bulk, (b) the disk-like GaN dots with height of 6.6, 7.1, and 8.2 nm.

Chapter 5 Conclusions

In this thesis, we have investigated the structural and optical properties of self-organized disk-like GaN dots grown on $Al_{0.11}Ga_{0.89}N$/sapphire by metal organic chemical vapor deposition (MOCVD) by means of atomic force microscopy (AFM) and photoluminescence (PL) spectroscopy. AFM studies show that for GaN coverage of 1.8 and 5.5 MLs, no island formation was observed. As the GaN coverage was increased above 7.3 MLs, self-organized GaN dots started to form, which is a typical characteristic of the Stranski-Krastanow (S-K) growth mode. And the wetting layer (WL) thickness is estimated to be about 7.2 MLs from the dependence of the dot density on the GaN coverage. The disk-like dot size varies with the GaN coverage, which was estimated from the TMGa flow rate. We knew that average height was about 5.7 to 8.2 nm and the standard deviation was about 2.1 to 2.8 nm from the histograms of dot height distribution with different GaN coverage. The average diameter was about 175 to 215 nm. The linear increasing of dot size with the increasing of the GaN coverage was observed. The estimated dot density is about $9.1x10^8$, $1.1x10^9$, $7.2x10^8/cm^2$ for the GaN coverage of 9.1, 10.9, 13.6 MLs, respectively. When the GaN coverage exceeded 13.6 MLs, the decrease in dot density is attributed to the coalescence of dots. From the morphologies observation of single disk-like GaN dot, we can classify the shape of single disk-like dot into symmetric and irregular types, where the symmetric type is divided into the lens-like and ellipse-like types. We consider that the ellipse-like GaN dot is likely made up of two smaller dots which was evidenced from the profile of the morphology.

We observed that the peak energy of the disk-like GaN dots increase with the decreasing GaN coverage from the PL measurement. It has been found that the disk-like GaN dots exhibited blueshift of 36 to 62 meV compared with GaN epilayers at room

temperature. The increasing of the transition energy with decreasing dot size is ascribed to the quantum size effect in the growth direction. Moreover, we observed that the FWHM of the disk-like GaN dots increases as the temperature increases. This is due to the increasing carrier-phonon scattering. It is also found that the increasing of the FWHM with the decreasing GaN coverage is attributed to the increasing size fluctuation.

We have also investigated the temperature dependence of PL properties of self-organized disk-like GaN dots with height ranging from 6.6 to 8.2 nm. The temperature dependence of GaN dots exciton emission and linewidth does not show any typical temperature dependent properties of the Stranski-Krastanow dots. The PL peak energy of the disk-like GaN dots exhibits an initial blue-shift with increasing temperature and then followed by a red-shift which obeys the Vashini's relation. The strength of blue-shifts increases with dot size. Such an energy shift with increasing temperature is a signature of QDs grown by SK growth mode and has also been observed in other QDs systems except for GaN QDs. This is a typical characteristic of the exciton localization. The localization energy of 5 meV for GaN epilayer is ascribed to the donor-bound exciton. However, the localization energy of 6 to 28 meV for disk-like dots is considered to exciton localization of defect state in the dots. In addition, the temperature dependent PL integrated intensity of GaN dots is analyzed by the Arrhenius equation. We can obtain the activation energies of 43±4, 70±13, and 106±13 meV for 6.6, 7.1, and 8.2 nm dots, respectively. From the PL spectrum of an $Al_{0.11}Ga_{0.89}N$ epilayer, the two peaks are contributed to the NBE and defect-related emissions. We found that the energy difference between I_{defect} of AlGaN and I_{QD} is close to the obtained activation energy. Finally, we suggest that the activation energy is the required energy of excitons from the QD confined state thermalized into defect states of AlGaN layers.

References

[1] A. J. Fischer, W. Shan, J. J. Song, Y. C. Chang, R. Horning, and B. Goldenberg, *Appl. Phys. Lett.* 71, 1981 (1997).

[2] Annamraju Kasi Viswanath, Joo In Lee, Sungkyu Yu, Dongho Kim, Yoonho Choi, and Chang-hee Hong, *J. Appl. Phys.* 84, 3848 (1998).

[3] Liwu Lu, Hua Yan, C L Yang, Maohai Xie, Zhanguo Wang, J Wang and Weikun Ge, *Semicond. Sci. Technol.* 17, 957 (2002).

[4] J. Bai, M. Dudley, L. Chen, B. J. Skromme, B. Wagner, R. F. Davis, U. Chowdhury and R. D. Dupuis, *J. Appl. Phys.* 97, 116101 (2005).

[5] S. Nakamura, M. Senoh, and T. Mukai, *Jpn. J. Appl. Phys.*, Part 2 32, L8 (1993).

[6] S. Nakamura, T. Mukai, and M. Senoh, *Appl. Phys. Lett.* 64, 1686 (1994).

[7] S. Nakamura and T. Mukai, Jpn. *J. Appl. Phys*., Part 2 31, L1457 (1992).

[8] S. Nakamura, T. Mukai, M. Senoh, and N. Isawa, *Jpn. J. Appl. Phys.*, Part 2 31, L139 (1992).

[9] S. Nakamura, M. Senoh, S. I. Nagahama, N. Isawa, T. Yamada, T. Matsushita, H. Kiyoku and Y. Sugimoto, *Jpn. J. Appl. Phys*., Part 2 35, L74 (1996).

[10] S. Chichibu, T. Azuhata, T. Sota, and S. Nakamura, *J. Appl. Phys*. 79, 2784 (1996).

[11] Y. Kawakami, Z. G. Peng, Y. Narukawa, S. Fujita, S. Fujita, and S. Nakamura, *Appl. Phys. Lett.* 69, 1414 (1996).

[12] S. Chichibu, A. Shikanai, T. Azuhata, T. Sota, A. Kuramata, K. Horino, and S. Nakamura, *Appl. Phys. Lett.* 68, 3766 (1996).

[13] A. Shikanai, T. Azuhata, T. Sota, S. Chichibu, A. Kuramata, K. Horino, and S. Nakamura, *J. Appl. Phys*. 81, 417 (1997).

[14] S. Nakamura, S. Masayuki, S. Nagahama, N. Iwasa, T. Yamada, T. Matsushita, Y. Sugimoto, and K. Hiroyuki, *Appl. Phys. Lett.* 70, 1417 (1997).

[15] M. A. Khan, J. N. Kuznia, A. R. Bhattarai, and D. T. Olson, *Appl. Phys. Lett.* 62, 1786 (1993).

[16] M. A. Khan, A. Bhattarai, J. N. Kuznia, and D. T. Olson, Appl. Phys. Lett. 63, 1214 (1993).

[17] M. Razeghi, and A. Rogalski, *J. Appl. Phys.* 79, 7433 (1996).

[18] Y. Arakawa and H. Sakaki, *Appl. Phys. Lett.* 40, 939 (1982).

[19] Y. Arakawa, T. Someya, and K. Tachibana, IEICE Trans. Electron. E83-C, 564 (2000).

[20] I. N. Stranski and V. L. Krastanov, Akad. Wiss. Lit. Mainz Abh. Math. Naturwiss. Kl. 146, 797 (1939).

[21] Wen-Cheng KE, Huai-Ying HUANG, Ching-Shun KU, Kao-Hsi YEN, Ling LEE, Wei-Kuo CHEN, Wu-Ching CHOU, Ming-Chih LEE, Wen-Hsiung CHEN, Wen-Jen LIN, Yi-Cheng CHENG and Ya-Tong CHERNG, *Jpn. J. Appl. Phys.* 43 L780 (2004).

[22] S. Guha, A. Madhukar, and K. C. Rajkuma, *Appl. Phys. Lett.* 57, 2110 (1990).

[23] S. Varma, C. M. Reaves, V. Bressler-Hill, S. P. Den Baars, and W. H. Weinberg, *Surf. Sci.* 393, 24 (1997).

[24] K. Kamath, P. Bhattacharya, T. Sosnowski, T. Norris, and J. Phillips, *Electron. Lett.* 32, 1374 (1996).

[25] R. Mirin, A. Gossard, and J. Bowers, *Electron. Lett.* 32, 1732 (1996).

[26] D. Bimberg, N. N. Ledentsov, M. Grundmann, N. Kirstaedter, O. G. Schmidt, M. H. Mao, V. M. Ustinov, A. Yu Egorov, A. E. Zhukov, P. S. Kopev, Zh. I. Alferov, S. S. Ruvimov, U. Gösele, and J. Heydenreich, *Jpn. J. Appl. Phys.*, Part 1 35, 1311 (1996).

[27] Q. Xie, A. Kalburge, P. Chen, and A. Madhukar, *IEEE Photonics Technol. Lett.* 8, 965 (1996).

[28] F. Widmann, B. Daudin, G. Feuillet, Y. Samson, J. L. Rouviere, and N. Pelekanos, *J. Appl. Phys.* 83, 7618 (1998).

[29] F. Widmann, J. Simon, B. Daudin, G. Feuillet, J. L. Rouviere, N. T. Pelekanos, and G. Fishman, *Phys. Rev. B* 58, R15989 (1998).

[30] B. Daudin, F. Widmann, G. Feuillet, Y. Samson, M. Arlery, and J. L. Rouvie`re, *Phys. Rev. B* 56, R7069 (1997).

[31] Koji Kawasaki, Daisuke Yamazaki, Atsuhiro Kinoshita, Hideki Hirayama, Kazuo Tsutsui and Yoshinobu Aoyagi, *Appl. Phys. Lett.* 79, 2243 (2001).

[32] M. Miyamura, K. Tachibana, and Y. Arakawa, *Appl. Phys. Lett.* 80, 3937 (2002).

[33] P. Ramval, S. Tanaka, S. Nomura, P. Riblet, and Y. Aoyagi, *Appl. Phys. Lett.* 73, 1104 (1998).

[34] P. Ramval, P. Riblet, S. Nomura, Y. Aoyagi, and S. Tanaka, *J. Appl. Phys.* 87, 3883 (2000).

[35] V. J. Leppert, C. J. Zhang, H. W. H. Lee, I. M. Kennedy, and S. H. Risbud, *Appl. Phys. Lett.* 72, 3035 (1998).

[36] E. Borsella, M. A. Garcia, G. Mattei, C. Maurizio, P. Mazzoldi, E. Cattaruzza, F. Gonella, G. Battagin, A. Quaranta, and F. D'Acapito, *J. Appl. Phys.* 90, 4467 (2001).

[37] E. Martinez-Guerrero, C. Adelmann, F. Chabuel, J. Simon, N. T. Pelekanos, G. Mula, B. Daudin, G. Feuillet, and H. Mariette, *Appl. Phys. Lett.* 77, 809 (2000).

[38] B. Daudin, G. Feuillet, H. Mariette, G. Mula, N. Pelekanos, E. Molva, J. L. Rouviere, C. Adelmann, E. Martinez-Guerrero, J. Barjon, F. Chabuel, B. Bataillou, and J. Simon, *Jpn. J. Appl. Phys.,* Part 1 40, 1892 (2001).

[39] A. D. Andreev and E. P. O'Reilly, *Phys. Rev. B* 62, 15851 (2000).

[40] V. A. Fonoberov, E. P. Pokatilov, and A. A. Balandin, *J. Nanosci. Nanotechnol.* 3, 253 (2003).

[41] Vladimir A. Fonoberov and Alexander A. Balandin, *J. Appl. Phys.* 94, 7178 (2003).

[42] D. Leonard, K. Pond, and P. M. Petroff, *Phys. Rev. B* 50, 11687 (1994).

[43] A. Y. Polyakov, M. Shin, J. A. Freitas, M. Skowronski, D. W. Greve, and R. G. Wilson, *J. Appl. Phys.* 80, 6349 (1996).

[44] Z. Y. Xu, Z. D. Lu, X. P. Yang, Z. L. Yuan, B. Z. Zheng, J. Z. Xu, W. K. Ge, Y. Wang, J. Wang, and L. L. Chang, *Phys. Rev. B* 54, 11528 (1996).

[45] P. Ramvall, S. Tanaka, S. Nomura, P. Riblet, and Y. Aoyagi, *Appl. Phys. Lett.* 73, 1104 (1998).

[46] Y. P. Varshni, *Physica* (Amsterdam) 34, 149 (1967).

[47] Y. T. Dai, J. C. Fan, Y. F. Chen, R. M. Lin, S. C. Lee, and H. H. Lin, *J. Appl. Phys.* 82, 4489 (1997).

[48] M. Leroux, N. Grandjean, B. Beaumont, G. Nataf, F. Semond, J. Massies, and P. Gibart, *J. Appl. Phys.* 86, 3721 (1999).

[49] C. S. Yang, Y. J. Lai, W. C. Chou, W. K. Chen, M. C. Lee, M. C. Kuo, J. Lee, J. L. Shen, D. J. Jang, and Y. C. Cheng, *J. Appl. Phys.* 97, 033514 (2005).

[50] M. Funato, A. Balocchi, C. Bradford, K. A. Prior, and B. C. Cavenett, *Appl. Phys. Lett.* 80, 443 (2002).

[51] Annamraju Kasi Viswanath, Joo In Lee, Sungkyu Yu, Dongho Kim, Yoonho Choi and Chang-hee Hong, *Appl. Phys. Lett.* 84, 3848 (1998).